Progress in Oceanography 177 (2019) 101943

Contents lists available at ScienceDirect

Progress in Oceanography

journal homepage: www.elsevier.com/locate/pocean

Seasonal variation of zooplankton community structure and trophic position in the Celtic Sea: A stable isotope and biovolume spectrum approach

Sarah L.C. Giering[a,*], Seona R. Wells[b,c], Kyle M.J. Mayers[d], Hanna Schuster[e], Louise Cornwell[f], Elaine S. Fileman[f], Angus Atkinson[f], Kathryn B. Cook[c], Calum Preece[e], Daniel J. Mayor[a,b]

[a] National Oceanography Centre, Southampton SO14 3ZH, UK
[b] Institute of Biological and Environmental Sciences, University of Aberdeen, Aberdeen AB41 6AA, UK
[c] Marine Scotland Science, Marine Laboratory, 375 Victoria Road, Aberdeen AB11 9DB, UK
[d] Ocean and Earth Sciences, University of Southampton, Southampton SO14 3ZH, UK
[e] Earth, Ocean & Ecological Sciences, University of Liverpool, 4 Brownlow Street, L69 3GP, UK
[f] Plymouth Marine Laboratory, Prospect Place, The Hoe, Plymouth PL13DH, UK

ARTICLE INFO

Keywords:
Zooplankton biomass
Zooplankton community composition
Trophic position
Biovolume spectra
Seasonal cycle

Regional index terms:
Celtic Sea
Northwest European Shelf

ABSTRACT

Zooplankton on continental shelves represent an important intermediary in the transfer of energy and matter from phytoplankton to the wider ecosystem. Their taxonomic composition and trophic interactions with phytoplankton vary in space and time, and interpreting the implications of this constantly evolving landscape remains a major challenge. Here we combine plankton taxonomic data with the analysis of biovolume spectra and stable isotopes to provide insights into the trophic interactions that occur in a shelf sea ecosystem (Celtic Sea) across the spring-summer-autumn transition. Biovolume spectra captured the seasonal development of the zooplankton community well, both in terms of total biomass and trophic positioning, and matched trophic positions estimated by stable isotope analysis. In early April, large microplankton (63–200 μm) occupied higher trophic positions than mesozooplankton (> 200 μm), likely reflecting the predominance of nanoplankton (2–20 μm) that were not readily available to mesozooplankton grazers. Biomass and number of trophic levels increased during the spring bloom as elevated primary production allowed for a higher abundance of predatory species. During July, the plankton assemblage occupied relatively high trophic positions, indicating important links to the microbial loop and the recycling of organic matter. The strong correlation between biomass and community trophic level across the study suggests that the Celtic Sea is a relatively enclosed and predominantly energy-limited ecosystem. The progression of the zooplankton biomass and community structure within the central shelf region was different to that at the shelf-break, potentially reflecting increased predatory control of copepods by macrozooplankton and pelagic fishes at the shelf break. We suggest that the combination of size spectra and stable isotope techniques are highly complementary and useful for interpreting the seasonal progression of trophic interactions in the plankton.

1. Introduction

Shelf seas are important for ecology, fisheries and biogeochemistry (Sharples et al., this issue) and face growing pressure from anthropogenic activities as the world's population increases (Levin et al., 2015); ~40% of the global population lives within 100 km of the coast and depends upon shelf sea ecosystems for its wellbeing. The development and management of shelf sea ecosystems require a holistic understanding of the factors that influence the community structures of the resident organisms and the ecosystem functions (e.g. carbon export, nutrient regeneration, secondary production, etc.) and services (e.g. food production, climate regulation) that they provide. This broad-scale understanding is increasingly explored and developed using ecosystem models (Hyder et al., 2015), particularly at the shelf- (or larger) scale. Such models necessarily represent a compromise between the complexity of natural ecosystems and the need for computational efficiency. Complex communities of individual organisms are typically represented by classes that may be further refined by terms such as size or trophic position.

Zooplankton act as vectors transferring energy from primary production to higher trophic levels, and play a central role in the biogeochemical cycles of the ocean. On continental shelves, zooplankton play

* Corresponding author.
E-mail address: s.giering@noc.ac.uk (S.L.C. Giering).

https://doi.org/10.1016/j.pocean.2018.03.012

Available online 16 March 2018

a strong role in energy transfer to fish and carbon transfer to the benthos (Marquis et al., 2011). To properly represent the energy flows in marine ecosystems and develop management strategies, it is therefore necessary to account for variability in zooplankton dynamics and population structure (Friedland et al., 2012; Mitra et al., 2014). The critical role of zooplankton in the marine environment requires models that accurately and sufficiently capture their dynamics (Everett et al., 2017), as the parameterization of zooplankton in many ecosystem models is very sensitive (Carlotti and Poggiale, 2010; Edwards and Yool, 2000; Heneghan et al., 2016). In many biogeochemical models, zooplankton are represented by 1–3 groups (Everett et al., 2017), typically spanning organisms ranging in size from small microzooplankton (> 0.002 mm) to krill or jellyfish (> 5000 mm).

Part of the difficulty in parameterizing zooplankton undoubtedly arises from the complexity of their communities. Zooplankton display enormous trophic plasticity that can change drastically over the course of a year as the community composition shifts. The seasonal development of an individual and/or a population is determined by a variety of external factors (e.g. nutrients, temperature, predation) and is also strongly linked to intrinsic cycles, such as reproductive cycles with generation times ranging from a few days to 1 year or more (Williams and Conway, 1982). Many zooplankton species change diet preferences during different seasons or ontogenetic stages, or display prey-switching behaviour (Sommer and Sommer, 2006; Stibor et al., 2004). Moreover, numerous species of microzooplankton are mixotrophic (Caron, 2016). The seasonal succession of phytoplankton (O'Boyle and Silke, 2010; Pingree et al., 1976) and the emergence of meroplanktonic species in shelf seas (Williams and Collins, 1986) further complicate zooplankton community dynamics. Zooplankton within a given size class or a broad group (e.g. microzooplankton vs. mesozooplankton) are thus unlikely to behave consistently through time and space, and models need to be able to deal with such plasticity.

Simple, static trophic positioning or broad grouping of zooplankton is thus difficult to apply, leading to conceptual models that misrepresent food chain structure with the trophic connections between large consumer species being much better understood and represented than those between e.g. microplankton species (Boyce et al., 2015). Boyce et al. (2015) hence argue that size-spectrum based modelling approaches are much more powerful in representing trophic connectivity and controls over plankton dynamics.

1.1. Trophic positioning

The trophic structures of ecosystems have traditionally been assessed using detailed knowledge of taxonomic composition and feeding strategies. However, detailed taxonomic analysis and determination of feeding strategies in zooplankton communities are notoriously difficult and laborious. Contemporary studies have therefore tended to adopt stable isotope (Minagawa and Wada, 1984) or size-based approaches (Basedow et al., 2010; Zhou, 2006) that are relatively quick and thus more amenable to the application at larger spatial and temporal scales.

The isotopic composition of an organism gives an indication of the trophic position and the food source: during feeding, animal body tissues become enriched in ^{15}N relative to its diet (Minagawa and Wada, 1984; Post, 2002a). Knowledge of the isotopic signature of the base of the food web (e.g. phytoplankton) and zooplankton thus allows the calculation of trophic positions.

An alternative method uses biomass spectra. Biomass spectra relate the total biomass of organisms of a certain size to its size class (Platt and Denman, 1977; Silvert and Platt, 1978). Size is an appealing trait to constrain ecosystem models because it is easily measured, scales with important processes like metabolism (Gillooly et al., 2001; Woodward et al., 2005) and food selectivity (Burns, 1968; Visser and Fiksen, 2013; Warren and Lawton, 1987), and constrains the role of organisms in the food web (Andersen et al., 2016; Blanchard et al., 2017). Thus, a seemingly simple measure can provide a great deal of information about the functioning of an organism and hence ecosystem dynamics if it is used beyond the simple grouping of a community according to size-fractions. Size-spectra further allow the calculation of trophic positions (Platt and Denman, 1977; Silvert and Platt, 1978). Empirical data have shown that the majority of biomass in an ecosystem is usually within small organisms, and the relative contribution to biomass decreases as an organism's size increases. The slope of a biomass spectrum can be interpreted with regard to respiration, growth, survival and mortality, and can give valuable insights into trophic relationships without the need for detailed taxonomic studies (e.g. Platt and Denman, 1977; Silvert and Platt, 1978; Zhou, 2006).

Biomass spectra and stable isotope analyses thus represent useful, integrative tools to assess the flows of energy and matter within an ecosystem (Zhou, 2006). Initial comparison between these two independent methods suggest that they are in general agreement with each other (Basedow et al., 2016; Tarling et al., 2012), although biovolume spectrum analysis has been suggested to detect higher levels of recycling than stable isotope analysis (e.g. in North Atlantic following the spring bloom) (Basedow et al., 2016). Moreover, comparison of the shape of biomass spectra combined with ecological data can give an insight into what controls ecosystem structure (Zhou et al., 2015).

As part of the UK Shelf Sea Biogeochemistry (SSB) Research Programme, we collected zooplankton to assess their abundance, biomass, taxonomic and elemental composition, and role in biogeochemical cycling in the Celtic Sea. Here we investigate the taxonomic and trophic changes of mesozooplankton communities at two contrasting sites in the Celtic Sea (mid-shelf and near the shelf break) along the seasonal succession (November 2014, April 2015 and July 2015). We further compare the trophic position estimates derived from two independent methods (bulk stable isotope measurements and biovolume spectra).

2. Methods

2.1. Study site

Zooplankton were collected during four periods (5–12th August 2014, 10–29th November 2014, 3–28th April 2015, and 13–31st July 2015) across the Celtic Sea (Southwest UK Shelf Sea) aboard RRS Discovery (cruises DY026, DY018, DY029 and DY033, respectively). We targeted three main stations (Fig. 1): the Shelf Edge site, which was located near the shelf break at the frequently studied site 'CS2' (48°34 N, 9°30 W; ~200 m water depth), the Central Site, which was located in the central Celtic Sea at a region with low fishing pressure and the SSB mooring ('CCS'; 49°25 N, 8°35 W; ~150 m water depth), and - when possible - within the 'Celtic Deep' area nearer to the coast (~51°10 N, 6°20 W; ~100 m water depth) . Note, owing to our limited data from the Celtic Deep, biomass and community composition are presented in the supplementary material only (Supplementary Fig. 1).

2.2. Sample collection

Samples for zooplankton biomass and elemental composition were sampled using WP2-size net rings (57 cm diameter) fitted with two different mesh sizes (63 μm and 200 μm). At each process station, WP2 nets fitted with non-filtering cod-ends and a closing mechanism were deployed during both daytime and night-time sampling from above and below the thermocline, and, when present, across the deep chlorophyll maximum (DCM; determined based on fluorescence). For the data analysis in this paper, we integrated across the water column. Table 1 provides the sampling details including net depths. The thermocline and DCM were determined from CTD casts immediately prior to the net deployments. The 63-μm and 200-μm mesh nets were hauled at $0.2\ m\ s^{-1}$ and $0.5\ m\ s^{-1}$, respectively. Collected zooplankton were fractionated using screens: a 200-μm mesh was used for screening of the organisms sampled with the 63-μm mesh net to retain the 63–200 μm

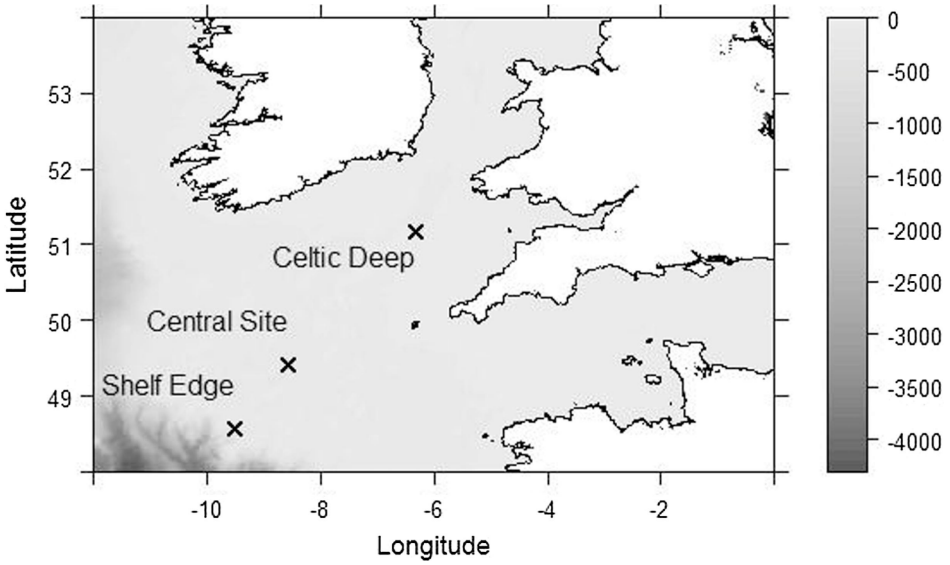

Fig. 1. Map of the Celtic Sea. Crosses indicate the three study sites. Grey scale shows bathymetry (in m).

fraction hereafter defined as "microplankton" (μP). A 500-μm mesh was used for the 200-μm mesh catch to separate the fractions 200–500 μm (defined here as "small mesozooplankton" smZ) and > 500 μm ("large mesozooplankton" lmZ) (Table 2). Each size fraction was split using a Folsom splitter: half was preserved in 4% borax-buffered formaldehyde for determination of community composition, directly measured dry

Table 1
Net deployment details.

Season	Site	Date	First net opened[a]		Depth horizon (in m)		
			Day	Night	Shallow	DCM[b]	Deep
August	Central Site	05/08/2014	13:41	21:29	0–30		30–120
	Shelf Edge	07/08/2014	07:08	20:50	0–50		50–120
	Celtic Deep	09/08/2014	07:35	–	0–50		50–95
	Celtic Deep	11/08/2014	16:00	20:35	0–50		50–90
	Celtic Deep	12/08/2014	08:49	20:40	0–40		40–100
November	Central Site	10/11/2014	14:01	20:24	0–50		50–130
	Central Site	12/11/2014	13:31	03:11	0–50		50–130
	Shelf Edge	17/11/2014	14:06	18:20	0–55		55–150
	Shelf Edge	19/11/2014	15:37	06:06	0–55		55–150
	Central Site	25/11/2014	14:02	20:55	0–60		60–130
	Celtic Deep	28/11/2014	–	21:56	0–70		70–100
Early April	Central Site	04/04/2015	16:19	23:59	0–80		80–120
	Central Site	05/04/2015	16:20	00:06[+]	0–60		60–140
	Shelf Edge[*]	08/04/2015	NA	22:20	0–120		120–200
	Shelf Edge	09/04/2015	16:31	21:55	0–60		60–150
	Central Site	10/04/2015	NA	21:38	0–60		60–120
	Central Site	11/04/2015	15:20	21:34	0–50		50–120
	Central Site	15/04/2015	14:12	21:27	0–20		20–120
	Central Site	16/04/2015	11:24	20:04	0–40		40–120
Late April	Central Site	20/04/2015	14:15	21:00	0–50		50–120
	Central Site	21/04/2015	11:16	20:20	0–50		50–120
	Shelf Edge	24/04/2015	14:19	NA	0–50		50–120
	Central Site	25/04/2015	14:12	21:44	0–50		50–120
	Central Site	28/04/2015	NA	00:17	0–50		50–120
July	Central Site	13/07/2015	13:40	23:50	0–60		60–120
	Central Site	14/07/2015	13:33	21:46	0–30	30–70	70–120
	Shelf Edge	19/07/2015	12:11	22:00	0–10	10–60	60–150
	Shelf Edge	20/07/2015	12:11	22:08	0–10	10–60	60–150
	Central Site	25/07/2015	12:43	NA	0–30	30–70	70–130
	Central Site	29/07/2015	12:23	22:02	0–30	30–50	50–130
	Central Site	30/07/2015	12:29	22:26	0–30	30–70	70–130

[a] Depth horizons were sampled using WP2-size net rings fitted with two different mesh sizes (63 μm and 200 μm) and a closing mechanisms. For each day or night profile 4–6 nets were deployed. Only the time of the first net opening is stated. Day and night time was determined based on the local photoperiod.

[b] Deep Chlorophyll Maximum was samples when present.

[+] Sampled on the 06/04/2015.

[*] Sampled at 48°25 N 9°53 W.

Table 2
Size fractions.

Group		Size fraction (µm)	Sampling method (and mesh size)	Preservation	Analysis tool	Direct dry weight measurements
Microplankton *	µP	63–200	Net (63 µm)	Formaldehyde	FlowCAM	No
Small mesozooplankton	smZ	200–500	Net (200 µm)	Formaldehyde	ZooScan	Yes
Large mesozooplankton	lmZ	> 500	Net (200 µm)	Formaldehyde	ZooScan	Yes

* Samples also contained detritus, faecal pellets and eggs. These are not considered µP.

weight (DW_m) and organic carbon (POC, $\delta^{13}C$) and nitrogen (PON, $\delta^{15}N$) content; the remainder was frozen at −80 °C for later analysis if desired.

2.3. Sample analysis, FlowCAM and ZooScan

Sub-samples (10–20 mL) of the µP samples were analysed using a FlowCAM VS-IVc (Fluid Imaging Technologies Inc.) fitted with a 300-µm path length flow cell, and a 4x microscope objective. Images were collected using auto-image mode at a rate of 6–12 frames per second. Image files were manually classified to determine the abundance of protists and metazoa using Visual spreadsheet software (Version 3.2.3).

SmZ and lmZ samples were split using a Folsom splitter until the aliquot contained ~1000 individuals (on average two splits). Aliquots were processed with a ZooScan (Biotom, Hydroptic, France) following the methods by Gorsky et al. (2010). Briefly, the scanning area of the ZooScan was filled with water, the scanning frame was inserted avoiding any bubbles being trapped under the frame, the sample was carefully poured into the scanning frame, and all individuals separated using a fine wooden pick. The sample was scanned at 2400 dpi resolution and captured using VueScan (version 8.3.23). A blank background image for background subtraction was taken before the first scan and after every fourth scan thereafter.

Scanned images were processed using ZooProcess (version 7.19) and Plankton Identifier (version 1.3.4) as described by Gorsky et al. (2010). Briefly, the software subtracts the proximate background image, and extracts and measures all objects. A training set was then built by sorting 1587 vignettes into 33 categories (including categories for unwanted objects such as fibres and detritus) and used to predict broadly the identity of the extracted objects. All predictions were manually validated and, if necessary, corrected. Object size was converted from pixel to millimetre by assuming a ratio of 0.0106 mm/pixel according to the scan resolution (Grosjean et al., 2004).

After scanning, individuals were recovered using a 50-µm mesh dish, transferred into pre-weighed tin cups (Elemental Microanalysis Ltd.), dried at 70 °C for 24 h, and weighed twice (ME5 or AE163 & AG135, Sartorius, Germany). Dried tin cups were re-weighed to obtain DW_m. The POC/PON concentrations and stable isotope signatures (δ, ‰) of the samples were determined using a Flash EA 1112 Series Elemental Analyser connected via a Conflo III to a Delta^{PLUS} XP IRMS (Thermo Finnigan).

2.4. Body volume calculation

To generate biovolume spectra and convert to image-derived dry weight (DW_A), we calculated the diameter and body volume of individual organisms. To calculate organism dimensions, we chose an area-based approach using the measured area of an individual as a starting point. It is important to consider that when reporting '*Area*', the ZooScan output includes holes in the object, whereas the FlowCAM output excludes any holes in the object. To directly compare the two approaches, we used ZooScan's '*Area_exc*' information, which excludes any holes, and FlowCAM's '*Area* (ABD)'. The '*area*' is thus the combined area of all the pixels that are deemed part of the individual. The area-based diameter (ABD) is the diameter of the circle obtained by arranging these pixels in a solid circle.

We calculated the volume of an individual (V_{ind} in mm^3) with the following assumptions. (1) The body area of an individual (A_{ind} in mm^2) can be arranged as a circle and the circle's radius r calculated. (2) The volume of an individual is equivalent to a sphere with radius r. It follows that

$$V_{ind} = 4/3\pi\left(\frac{A_{ind}}{\pi}\right)^{3/2} \quad (1)$$

As only an aliquot of the net sample was imaged, we then calculated the total biovolume of this individual 'type' in the net sample (BV_{type} in mm^3 $sample^{-1}$) by taking into account the fraction of the sample that was analysed ($Frac_{Split}$ in $sample^{-1}$):

$$BV_{type} = \frac{V_{ind}}{Frac_{Split}} \quad (2)$$

All types were summed to give the biovolume of the community (BV_{comm} in mm^3 $sample^{-1}$). BV_{comm} was later used for the biomass spectra.

2.5. Dry weight (DW) calculation

DW based on the FlowCAM and ZooScan images (DW_A in mg ind^{-1}) was calculated following the regressions between body area of an individual (A_{ind} in mm^2) and its DW (Lehette and Hernández-León, 2009):

$$DW_{A\,ind} = a \times A_{ind}^{b} \times 1/1000 \quad (3)$$

where a and b are the coefficients. We used $a = 43.38$ and $b = 1.54$ for most groups as determined for 'general mesozooplankton' ($p < 0.001$, $R^2 = 0.95$). Chaetognaths do not fit this regression line, and we therefore used the coefficients $a = 23.45$ and $b = 0.84$ ($p < 0.001$, $R^2 = 0.84$) (Lehette and Hernández-León, 2009). Gelatinous zooplankton contain more water than crustacean zooplankton and their DW is therefore likely overestimated using these regressions. We tested three methods to estimate gelatinous DW from ZooScan images. (1) We used the coefficients determined for salps ($a = 4.03$, $b = 1.24$, $p < 0.001$, $R^2 = 0.90$) (Lehette and Hernández-León, 2009) for all gelatinous zooplankton (cnidarian, siphonophores, doliolids, salps and ctenophores), *Luidia sarsi*, polychaetes and pteropods. (2) We applied the coefficients determined for siphonophores to these groups ($a = 43.17$, $b = 1.02$, $p < 0.001$, $R^2 = 0.92$) (Lehette and Hernández-León, 2009). (3) We applied the coefficients for general mesozooplankton (see above) and assumed gelatinous zooplankton to have only 22% of the DW predicted for general zooplankton. The latter assumption was based on the observation that crustaceans and jellies contain 18% and 4% DW (%wet weight), respectively (Kiørboe, 2013). We found that the first method produced the best agreement with measured DW_m throughout all seasons and particular for November, when gelatinous zooplankton were most abundant. For November, the slopes of the linear regressions between ZooScan-based DW_A and measured DW_m at the Central Site were 0.45 ($p = 0.03$, $R^2 = 0.67$), 0.27 ($p = 0.04$, $R^2 = 0.60$) and 0.25 ($p = 0.06$, $R^2 = 0.54$) for the three methods, respectively. Overall, ZooScan-based DW_A and measured DW_m for all stations agreed well ($DW_m = 0.89 \pm 0.04\ DW_A + 0.07 \pm 0.24$; $p < 0.01$, $R^2 = 0.92$, $n = 46$; Fig. 2).

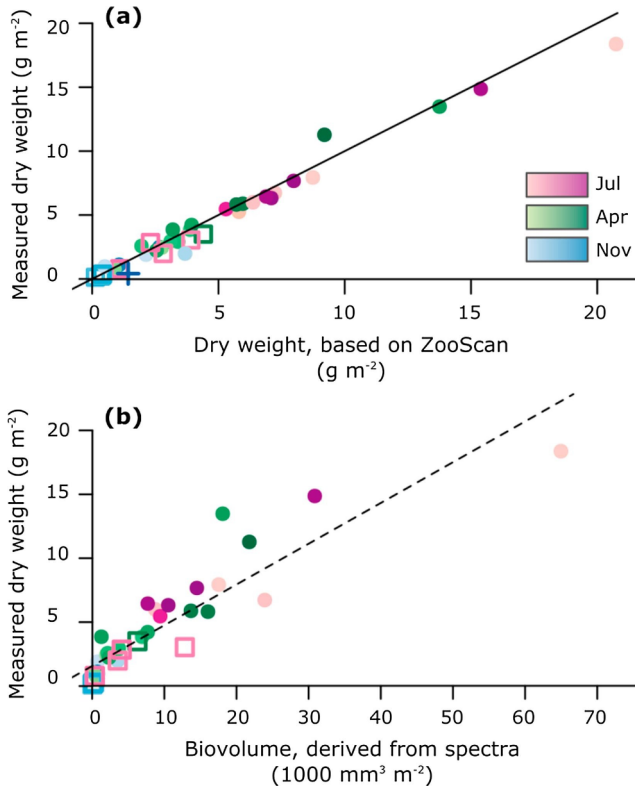

Fig. 2. Relationship between ZooScan-based biomass and measured biomass. **(a)** ZooScan-based dry weight vs. measured dry weight (see Section 2.6). Linear regression: $y = 0.89x + 0.07$ ($p < 0.01$; $R^2 = 0.92$, n = 46). **(b)** Biovolume calculated from biovolume spectra vs. measured dry weight (see Section 2.7). Linear regression: $y = 0.32x + 1.57$ ($p < 0.01$; $R^2 = 0.82$, n = 43). Points are coded according to sampling location (circle: Central Site; square: Shelf Edge; cross: Celtic Deep) and sampling month (see legend).

Integrated DW_A (DW_{A_int} in mg DW m^{-2}) was calculated by summing all individuals (DW_A in mg ind^{-1}), taking into account the fraction of the sample that was analysed and the area of the net (A_{net} in m^2):

$$DW_{A,int} = \frac{\sum DW_{A,ind}}{Frac_{Split} \times A_{net}} \quad (4)$$

2.6. Biovolume spectra

Biovolume spectra, which are analogous to biomass spectra, can be computed when information is available about size (Basedow et al., 2010 and Refs. herein). We here computed biovolume spectra for all water column samples (i.e. above + below the thermocline, and where applicable including the DCM) by combining the data sets from the three size fractions (µP, smZ and lmZ). We created 100 biovolume size intervals (Δw in mm^3) logarithmically spaced between $w_{min} = 10^{-4}$ mm^3 and $w_{max} = 10^3$ mm^3 (equivalent spherical diameters, ESDs, of 0.06 and 12.4 mm, respectively). All individual 'types' (BV_{type} in mm^3 $sample^{-1}$; see Section 2.4) were sorted into these size intervals according to the type's volume (V_{ind} in mm^3). For example, a dinoflagellate with a V_{ind} of 0.00011 mm^3 ($10^{-3.96}$) would be sorted into the first size interval (Δw_1 with range $10^{-4.00}$ to $10^{-3.93}$). We included detritus, faecal pellets and eggs, as these can be utilized within the food web. The normalized biovolume in each size interval ($b_{\Delta wx}$ in m^{-3}) was then calculated as:

$$b_{\Delta w_x} = \frac{\sum (BV_{type} in \Delta w_x)}{\Delta w_x} \times \frac{1}{A_{net} \times z_{max}} \quad (5)$$

where Δw_x is the width of a size interval in mm^3 (i.e. upper boundary in mm^3 minus lower boundary in mm^3), A_{net} is the area of the net (in m^2), and z_{max} is the depth of the sampled water column (in m). The biomass spectrum was computed by plotting all $b_{\Delta wx}$ against the midpoint of their respective intervals, $\overline{w}_x$. In case of the first size interval (Δw_1 with range $10^{-4.00}$ to $10^{-3.93}$), $\overline{w}_1 = (10^{-4.00} + 10^{-3.93})/2$. Finally, linear regressions were fitted to the $\log_{10}$-$\log_{10}$ transformed data to derive slopes and intercepts of the biovolume spectra.

We calculated slopes and intercepts for µP, smZ, lmZ and the whole assemblage (µP + smZ + lmZ). The size cut-off for these groups was based on the mesh sizes for fractionation (63, 200, 500 and 2000 µm). These mesh sizes were treated as diameter and converted into volume following Eq. (1), giving $10^{-3.88}$, $10^{-2.38}$, $10^{-1.18}$ and $10^{0.62}$ mm^3, respectively. Linear regressions were then fitted to the size ranges according to Table 2. For example, to derive slope and intercept for µP, we fitted a linear regression to the biovolume spectrum between $\overline{w}_x = 10^{-3.88}$ and $\overline{w}_x = 10^{-2.38}$.

We further calculated the biovolume of the whole assemblage using the slope and intercept of the entire biovolume spectra (10^{-4} to 10^3 mm^3) and integrating underneath the line. The calculated biovolume (BV) was strongly correlated with integrated biomass directly measured from the net samples, with a regression equation of DW_m (in g DW m^{-2}) $= 0.32 \pm 0.02$ BV (1000 mm^3 m^{-2}) $+ 1.57 \pm 0.32$ ($p < 0.01$; $R^2 = 0.82$, n = 43; Fig. 2b).

2.7. Trophic position

Trophic position based on biovolume spectra (TP_{BVS}) was calculated following Zhou (2006) as

$$TP_{BVS} = -\frac{1 + cAE}{cAE \times m} \quad (6)$$

where cAE is the community assimilation efficiency (with $cAE = 0.7$ (Zhou, 2006)) and m is the slope of the biomass spectrum (note the $\log_{10}$-$\log_{10}$ transformation). TP_{BVS} can be calculated for the entire population or for individual size classes. A TP = 1 represents primary producers, whereas TP = 2 and TP = 3 represent approximately primary and secondary consumers, respectively. Higher TPs can either suggest a higher proportion of carnivores or a higher level of recycling through the microbial loop (Basedow et al., 2016). To better constrain the uncertainties in this calculation, we explored the sensitivity of calculated TP to variability in cAE. There is no direct measurement of cAE, but we can assume that the average of assimilation efficiency of all plankton should be equivalent to the cAE (Zhou, 2006). A wide range of assimilation efficiencies has been reported in the literature, ranging from < 0.10 to 0.96, though most reported values range from around 0.50–0.90 (Steinberg and Landry, 2017). We used this latter range and calculated TP for slopes ranging from −0.4 to −1.0 (our observed range).

We further calculated TP based on isotopes of nitrogen ($\delta^{15}N$). One of the biggest difficulties of this method is to identify an isotopic baseline ($\delta^{15}N$ of primary producers). We used the isotopic composition of particulate organic matter as a baseline. Samples for the analysis of particulate nitrogen isotopes were collected from the upper 50 m of the water column (encompassing the surface mixed layer depth; Poulton et al., this issue). ≥1 L of unscreened seawater was filtered onto precombusted (450 °C) grade F glass fibre filters (Whatman GF/F, 25 mm diameter, nominal pore size 0.7 µm), and stored frozen at −80 °C until analysis. The filters were freeze-dried and then pelletized using tin capsules. Stable N isotope analysis was carried out using an Elemental Analyser (Costech Instruments) interfaced with an IRMS (Thermo Finnigan). Isotope ratios are reported using delta notation (δ) with units per mil (‰) as above. Samples were calibrated using internationally recognized standards, USGS40 (δ15N = −4.5‰ (Qi et al., 2003)), USGS41 (δ15N = +47.6‰ (Qi et al., 2003)), IAEA-N-1 (δ15N = +0.4‰ (Gonfiantini, 1978)), and IAEA-N-2 (δ15N = +20.3‰ (Gonfiantini, 1978)). TP based on isotopes (TP_{iso})

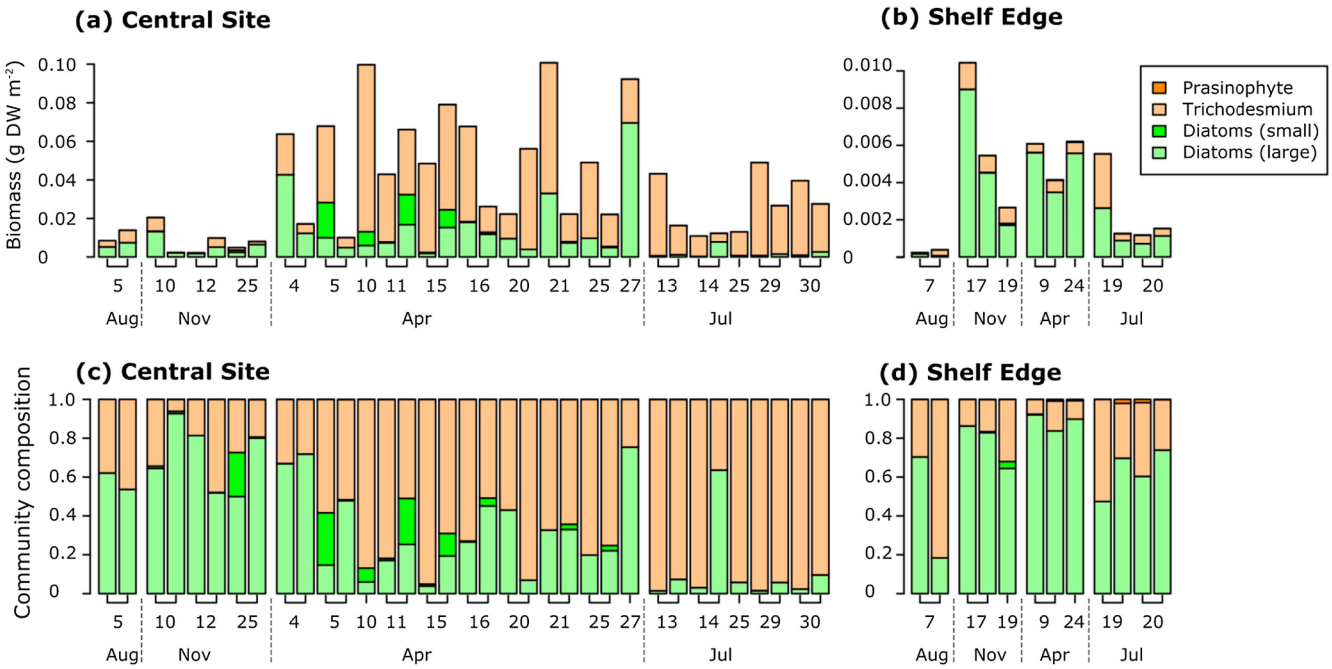

Fig. 3. Biomass and composition of autotrophic microplankton in the 63–200 µm fraction at the Central Site **(a,c)** and the Shelf Edge **(b,d)** throughout the study as determined by FlowCAM. Lower panels of these figures express the fraction of total dry weight. Please note that *Trichodesmium sp.* biomass is for trichomes in the 63-200 µm fraction, only. Total *Trichodesmium* biomass in the water column was likely much higher.

was then calculated as

$$TP_{iso} = \frac{\delta^{15}N_{zoo} - \delta^{15}N_{baseline}}{\varepsilon} + 1.5 \quad (7)$$

where $\delta^{15}N_{zoo}$ and $\delta^{15}N_{baseline}$ are the isotopic composition (in ‰) of the zooplankton (smZ or lmZ) and the particulate organic matter, respectively. We assumed an enrichment per TP (ε) of 3.4‰ (Post, 2002a) and that particulate organic matter was a mix of detritus, phytoplankton, microzooplankton and bacterioplankton, which in combination had a $TP_{baseline}$ of 1.5 (Sommer, 2004). As there was a marked enrichment in $\delta^{15}N$ of the particulate matter ($\delta^{15}N_{PON}$) throughout the year, we calculated TP using a seasonally variable baseline based on measurements at the Central Site during our cruises (0.0, 1.0, 2.8 and 4.6‰ for November, early April, late April and July, respectively).

We explore the limitations of both methods in the supplementary material (S.1). Overall, both trophic indices are associated with large uncertainties and results should therefore be interpreted with caution. Nevertheless, the two estimates (TP_{BVS} and TP_{iso}) for lmZ agreed reasonably well (Fig. 9), as previously reported (Tarling et al., 2012; Basedow et al., 2016).

2.8. Statistics

Plankton assemblages were analysed using multivariate ordination from the vegan package in R (Oksanen et al., 2016; R Core Team, 2015). Plankton were grouped into 41 groups (Supplementary Table 1). Bray-Curtis dissimilarities were calculated and visualised using non-metric multidimensional scaling (NMDS) with the metaMDS function. The biomass data were square-root transformed and submitted to Wisconsin double standardization to reduce the influence of groups with high biomass. Two dimensions were calculated with acceptable stress (< 0.2) (Legendre and Legendre, 1998). The solution was centred, rotated to present the largest variance along the first dimension, and scaled so that one unit corresponds to halving the similarity between two communities. For detailed explanations of the function see the metaMDS help package (Oksanen et al., 2016).

Relationships between plankton community structure and environmental parameters (longitude, year day, daytime, integrated Chlorophyll *a* (Chl), sea surface temperature and euphotic zone depth) were tested using the envfit function, which estimates the correlation and direction of forcing of environmental parameters within the NMDS state space. The significance of the correlation was assessed using 999 random permutations of the environmental variables.

The differences between *a priori* groups (e.g. between sites and/or seasons) were tested using non-parametric multivariate analysis of variance (PERMANOVA) (Anderson, 2001) using the adonis function with 999 random permutations. Data were transformed as described above and dissimilarity indices calculated using the vegdist function, which gives identical results to metaMDS but in a different data format. As significant differences identified by PERMANOVA can be due to either differences in location and/or differences in dispersion, we used the function betadisper, which is analogous to Levene's test, and the ANOVA-like permutation function permutes (with 999 random permutations) to test for differences in group homogeneities (Anderson et al., 2006).

The seasonal progression of TP_{bvs} and spectra-derived biovolume was determined using a smoothing function (cyclic cubic regression splines) from the mgvc package (Wood, 2017). This fit was for illustrative purposes only and, therefore, no further statistics were carried out.

3. Results

3.1. Overall deployments

A total of 246 net hauls were taken for biomass samples (Table 1), providing 44 vertical depth profiles. Diel vertical migration was observed for most paired day-night hauls. For this study, we integrated biomass across the water column, typically between 0 and 120 m at the Central Site and 0–150 m at the Shelf Edge. The complete data set (Giering et al., 2018) can be obtained from the British Oceanographic Data Centre (doi:10/cngc).

3.2. Microplankton (μP) biomass and community composition

We have no direct measurements of μP biomass but inferred their biomass from the FlowCAM images. The samples contained μP as well as detritus, faecal pellets and eggs. Overall, μP made up 60 ± 14% (0.01–0.11 g DW m^{-2}) of the estimated total biomass in the sample with the remaining biomass (40 ± 14%) being associated with detritus, faecal pellets and eggs. Of this 60%, photosynthesizing μP (diatoms, *Trichodesmium*, and prasinophytes) made up 23 ± 14%. At the Central Site, their biomass was lowest in August and November, and highest in April and July with up to 0.1 g DW m^{-2} (Fig. 3a). This increase was largely driven by *Trichodesmium* (Fig. 3b). It is important to note that these values for *Trichodesmium* are only semi-quantitative. *Trichodesmium* forms large colonies that are > 200 μm in diameter and are thus mechanically excluded from μP (63–200 μm fraction). Some of the individual trichomes will however pass through the 200-μm mesh during fractionation and contribute to μP biomass, which is what we report here. *Trichodesmium* biomass in the water column was likely substantially higher than suggested in Fig. 3, but the overall trend (i.e. increased abundance in April) is likely representative.

Heterotrophic μP made up on average 77 ± 14% of the μP biomass, with lowest values (~50%) in April at the Central Site. Heterotrophic μP biomass ranged from ~0.02 g DW m^{-2} in November to ~0.10 g DW m^{-2} in late April (Table 2; Fig. 4). There was a strong degree of similarity in the relative composition of the μP community at the Central Site and the Shelf Edge (Fig. 4), with differences being mostly driven by changes in the relative abundances of nauplii and dinoflagellates during November/April.

At the Central Site (Fig. 4a), nauplii biomass was highest in July, with a median contribution to the biomass of 47, 33, 61, 59 and 75% in August, November, early April, late April and July, respectively. Copepodites contributed 20–49% (49, 29, 20, 28 and 27% for the five periods, respectively). Dinoflagellates contributed most in November (median of 11%) and were less dominant in August, early April, late April and July (3, 11, 4 and 3%, respectively). Tintinnids and polychaetes were present all year round in this fraction. Tintinnids contributed moderately to large microzooplankton biomass (< 0. 1, 4, 4, 3 and < 0.1% in the five periods, respectively) but reached up to 10% of the biomass at some of the stations. Polychaetes contributed always < 2%. Ciliates in this size fraction were not observed in July and August, and were only occasionally observed during the other periods with always < 2% of μP biomass. Radiolaria were observed occasionally in November, late April and July (< 0.1%) and small appendicularians occasionally in April (< 3%). Other groups made up < 3% of μP biomass with the exception of the 12th November, where *Oithona* contributed 5% to μP biomass (Fig. 4a).

At the Shelf Edge (Fig. 4b), nauplii biomass was highest in late April with > 60% of μP biomass (median 32, 36, 52, 62 and 52% of the biomass in August, November, early April, late April and July, respectively). Copepodite contribution was relatively constant with 31–41% throughout the year (36, 39, 41, 31 and 32% for the five periods, respectively). Dinoflagellates contributed most in July (31% of μP biomass) and less in August, November, early and late April (19, 16, 5 and 6% respectively). Appendicularians were present all year round with < 2% of the biomass except for in November, where they contributed up to 12% of μP biomass (median: 3%). All other groups were observed occasionally. Tintinnid biomass was low (0, 3, < 1 and 1% in August, November, April and July, respectively). Polychaetes were not observed in early April, and made up < 1% of the biomass during the remaining periods. Ciliates were not observed in April, contributed < 1% in November and July, but contributed 11% to μP biomass in August. Radiolaria were not observed in August and late April, with small biomass during November and July (< 1%), and occasionally with high biomass in early April (range: 0–4%) (Fig. 4b).

3.3. Mesozooplankton (smZ and lmZ) biomass and community composition

Median biomass of mesozooplankton (heterotrophs > 200 μm) across all samples was 2.5 g DW m^{-2} (quartile range: 1.0–4.5 g DW m^{-2}) with the lowest biomass in November and early April, and highest biomass in late April and July (Table 2; Fig. 5). Mesozooplankton biomass at the Central Site was consistently higher than at the Shelf Break (Table 2). At the Central Site, total mesozooplankton biomass was 1.5, 2.7, 5.5 and 7.2 g DW m^{-2} in November, early April, late April

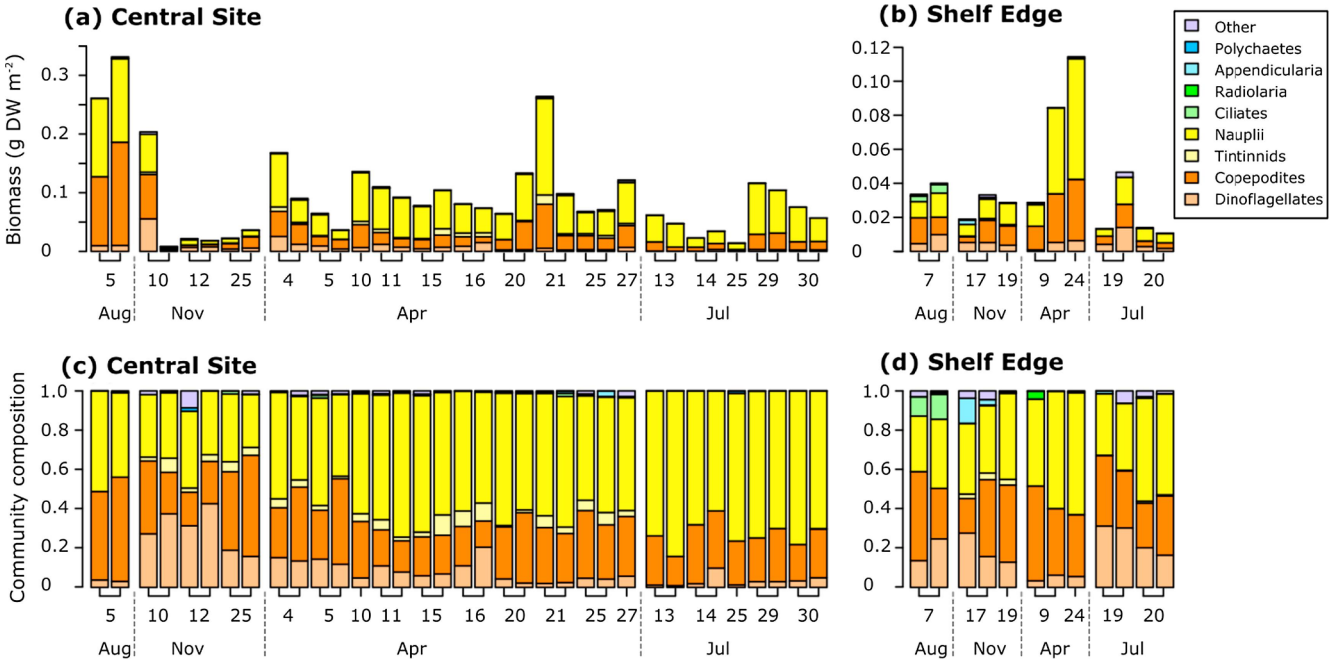

Fig. 4. Biomass and community composition of mixo- and heterotrophic microplankton in the 63–200 μm fraction based on FlowCAM at the Central Site (**a,c**) and the Shelf Edge (**b,d**). Grouped in'other' are foraminifera, flagellates, miscellaneous larvae, rotifers, silicoflagellates and *Oithona*, all ofwhich contributed ≤5% in all samples. Lower panels of these figures express the fraction of total dry weight. Note different scales on axes.

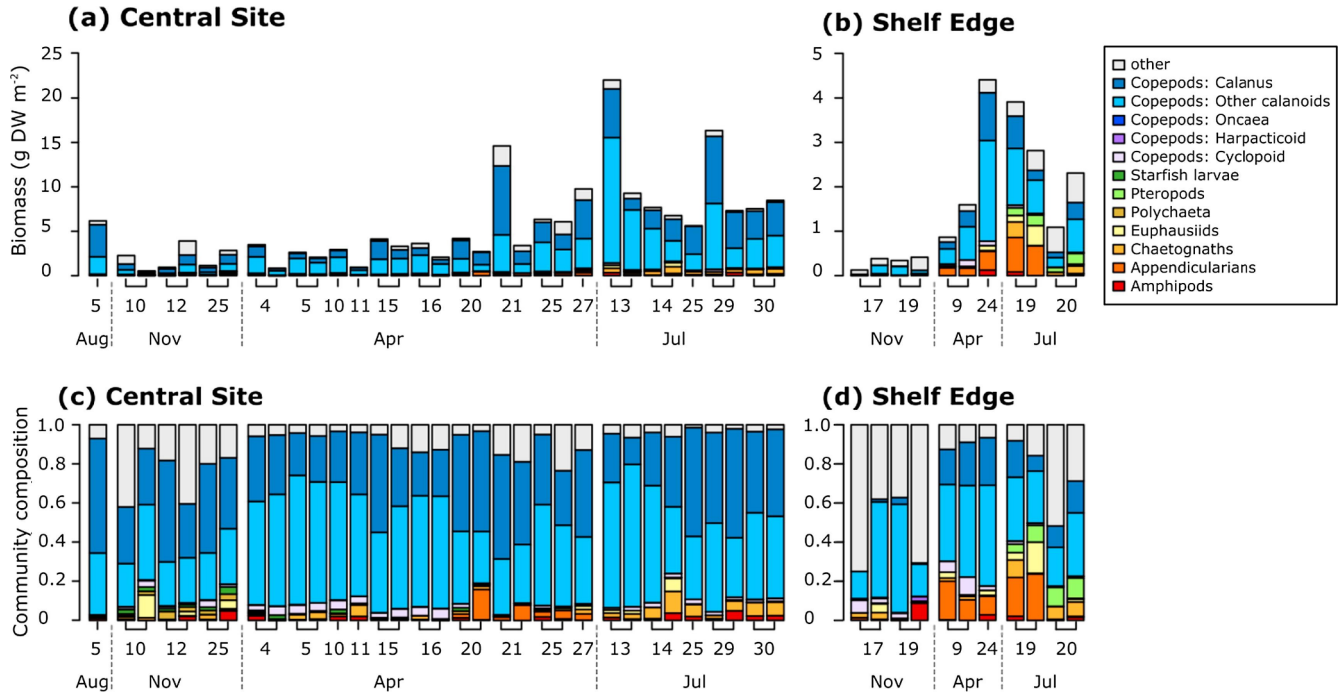

Fig. 5. Biomass and community composition (based on abundance) of mesozooplankton based on ZooScan at the Central Site (**a,c**) and the Shelf Edge (**c,d**). Grouped in 'other' are cladocerans, dinoflagellates, echinoderm, eggs, foraminifera, gymnosomata, unidentified larvae, nauplii, ostracods and radiolarian, all of which contributed < 3% in all samples. Lower panels of these figures express the fraction of total dry weight. Note different scales on axes.

Table 3
Zooplankton biomass (g DW m^{-2}) through the seasons 2014/2015. Early and late April refer to before and after the 19 April 2015. Values are median (quartile range).

Central Site	November	Early April	Late April	July
63–200*	0.02 (0.02–0.03)	0.09 (0.08–0.11)	0.10 (0.07–0.13)	0.06 (0.03–0.08)
200–500	0.2 (0.2–0.3)	1.1 (0.5–1.3)	1.7 (1.1–2.1)	2.7 (1.6–5.7)
> 500	1.2 (0.8–1.7)	1.5 (0.6–1.6)	3.7 (2.8–6.7)	4.4 (3.9–5.3)
Total biomass	1.5 (1.0–2.0)	2.7 (1.1–3.0)	5.5 (4.1–8.9)	7.2 (5.5–11.1)
Shelf Edge	**November**	**Early April**	**Late April**	**July**
63–200*	0.02 (0.01–0.03)	0.04 (0.04–0.07)	0.11 (N/A)	0.01 (0.01–0.02)
200–500	0.1 (0.1–0.1)	0.6 (0.4–0.8)	1.7 (N/A)	0.4 (0.3–0.4)
> 500	0.2 (0.1–0.2)	0.4 (0.3–0.4)	1.8 (N/A)	2.0 (1.4–2.4)
Total biomass	0.3 (0.2–0.3)	1.0 (0.8–1.2)	3.6 (N/A)	2.4 (1.7–2.9)

* Biomass of zooplankton in the 63–200 µm fraction was estimated from FlowCAM images.

and July, respectively. At the Shelf Break, the respective biomasses were 0.3, 1.0, 3.6 and 2.4 g DW m^{-2} (Table 2). At both sites, lmZ biomass was consistently higher than smZ biomass (Table 2). The carbon-to-DW ratio for both size fractions was relatively constant across all study periods (0.45–0.51 g C [g DW]$^{-1}$; see Table 3).

The community composition varied throughout the year. We here describe the overall community composition of both size fractions combined; plots of biomass and community composition for the individual fractions (smZ and lmZ) are provided in the supplementary material (Supplementary Figs. 2 and 3). Please note that all values are the median contribution to total DW_A biomass based on ZooScan. At the Central Site (Fig. 5a), copepods made up the bulk of the biomass during early April, late April and July (89%, 80% and 88%, respectively). In November, copepods still dominated (68%) but the community was more diverse. Gelatinous zooplankton made up ~9% of the biomass in November, and were present only as low biomass throughout the rest of the year (< 1%). Larvae of the starfish *Luidia sarsi* were also prevalent during November and early April (2% and < 1%, respectively), but not caught disappeared in July. Polychaetes were most common in November (2%), with little biomass in April (< 1%). They appeared again in July (< 1%). Amphipods and chaetognaths were present all year round (median of < 1%), but contributed most to total biomass in July (2 and 6%, respectively). Appendicularian biomass was low in November and early April (< 1%), and peaked in late April (3%). Euphausiids were around all year with relatively low biomass (< 1%). We did not find any pteropods at the Central Site.

At the Shelf Edge, the mesozooplankton community composition was very different compared to the Central Site (Fig. 5b). Gelatinous zooplankton dominated in November with up to 69% of the biomass (median: 38%). Copepods were the second most prevalent group in November with up to 62% (median: 37%) of the biomass. Copepods made up the bulk of the biomass in April (median of 70 and 78% in early and late April, respectively). In July, they contributed 31–53% (median 43%). Appendicularian biomass was low in November (< 1%), but contributed 15, 9 and 10% in early April, late April and July, respectively. In July, the Shelf Edge experienced a high biomass of pteropods, which contributed 9% of the biomass. The larvae of the starfish *L. sarsi* was only observed once in November (< 1%). Polychaetes were present all year round, albeit with low biomass (< 1%). Amphipods, chaetognaths and euphausiids were present all year, with maximum contributions of 9, 9, and 16% of the biomass, respectively. Median relative biomass for November, early April, late April and July respectively were < 1, < 1, 3 and 1% for amphipods, 2, 2, < 1 and 7% for chaetognaths, and < 1, 2, 3 and 3% for euphausiids.

3.4. Environmental drivers of community composition

The NMDS shows clear clustering of the different sites and seasons (Fig. 6). Plankton community structures were significantly correlated with longitude, day of year, integrated Chl and sea surface temperature (Table 4). Euphotic zone depth and time of day (i.e. night-time or daytime haul) did not explain the community grouping (Table 4).

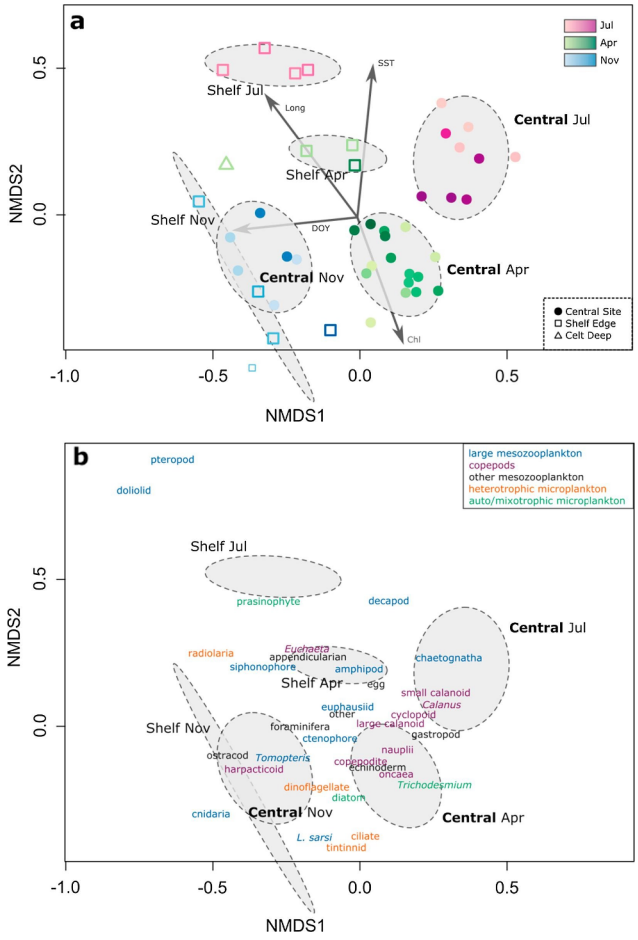

Fig. 6. Cluster analysis of plankton communities at the Central Site and the Shelf Break during November 2013, April 2014 and July 2014. Communities were analyzed using non-metric multidimensional scaling (NMDS) with an acceptable stress (0.17). Points closer together have higher similarity. **(a)** Each vertical profile is represented as a data point with colours and symbols according to month (see legend) and sampling location (solid circle: Central Site, square: Shelf Edge, triangle: CelticDeep). Grey ovals show confidence intervals of *a priori* groups (Central Site and Shelf Edge each during the three seasons). Arrows shows significant environmental explanatory variables: Sea surface temperature (SST), Chlorophyll *a* (Chl), Day of year (DOY) and Longitude (Long). **(b)** Graphical representation of species that are characteristic (in terms of relative abundance) for the vertical profiles as shown in panel a. Functional groups are represented by colour as shown in legend.

Community compositions were significantly different at different sites ($p < 0.001$) and in different months ($p < 0.001$). There was a weak interaction between the two factors ($p = 0.08$; Table 5). Pairwise *a posteriori* tests confirmed that differences were caused by different centroids rather than different dispersion (Anderson, 2001).

3.5. Trophic structure

We determined trophic positioning using biovolume spectra and stable isotope analysis for individual size classes (Fig. 7). Biovolume spectra for µP and lmZ yielded good fits ($R^2 > 0.77$), whilst fits to smZ were poor (median $R^2 = 0.28$). Moreover, smZ appeared to have a shallower biovolume spectrum slope compared to the other size classes. This is in line with observations from a study that compared biovolume spectra obtained from net samples analysed using ZooScan to those obtained using an *in situ* Laser Optical Plankton Counter (Schultes and Lopes, 2009). The authors suggest that only particles with a size of > 450 µm ESD are efficiently sampled by 200-µm mesh nets (see also Hopcroft et al., 2001), explaining a flattening of the slope for plankton < 500 µm. We therefore exclude smZ from the biovolume spectra discussion. A further complication arises from the use of two methods (FlowCAM vs ZooScan). Direct comparison of the results from the two methods has therefore to be viewed with caution. Nevertheless, we believe that data within each sampling method are robust, and slopes (i.e. trophic position) for any given method can therefore be readily compared.

Our sensitivity analysis shows that uncertainty in community assimilation efficiency has a relatively small effect on the trophic positions calculated from biovolume spectra. Trophic positions calculated from steep slopes (< −0.7) are more robust than those calculated from shallower slopes (> −0.7) (Supplementary Fig. 4). Across the tested range (slopes −1 to −0.4), the uncertainty was low at ± 0.3 TP (average difference between TP based on $cAE = 0.7$ and cAE ranging between 0.4 and 0.9; see Supplementary Material S.1).

Trophic positions estimated from biovolume spectra varied between size fractions and seasons (Fig. 8). At the Central Site, trophic positioning of the different size classes changed markedly throughout the year: median trophic position of µP compared to lmZ was lower in November (2.3 vs 4.7, respectively), higher in early April (3.3 vs 2.4, respectively), and similar in late April (3.6 vs 4.3) and July (2.8 vs 2.3, respectively). At the Shelf Edge, the trophic positions of the two size groups (µP vs lmZ) were similar in November, late April and July (respectively 2.2 vs 2.2, 2.5 vs 2.6, and 2.4 vs 2.8). However, in early April, the trophic position of µP was high with a median of 4.4, whereas the trophic position of lmZ was low with a median of 1.8.

Estimates of trophic position based on stable isotope analysis (TP_{iso}) of smZ ranged from 1.3 to 3.8 with lowest values in April and highest in November (Table 4). TP_{iso} of lmZ was generally slightly higher by 0.1–0.4 TPs compared to smZ (Table 4). Overall, TP_{iso} of lmZ agreed reasonably well with trophic position derived from biovolume spectra, except for samples collected in late April (Fig. 9). See Supplementary Material S.1 for a detailed uncertainty analysis.

Changes in community trophic position and biomass appeared to follow the same seasonal trend across the study sites (Fig. 10a and b). Indeed, zooplankton biomass (expressed either as the intercept of the biovolume spectra or as DW_m) was closely correlated to both slope and community trophic position (Fig. 10c and d). The slope m decreased steepness by 0.16 units per 10-fold increase in biovolume ($m = 0.16 \log_{10}(BV \text{ in mm}^3) - 1.16$; $p < 0.01$, $R^2 = 0.75$, $n = 43$). This translates to a community trophic position increase of 1.1 TP per 10-fold increase in biovolume (Fig. 10d).

4. Discussion

4.1. Seasonal community progression in the Celtic Sea

Our estimates of zooplankton biomass and composition matched previous records well: The long-term monthly mean mesozooplankton biomass suggests higher biomass on the shelf than at the shelf break (Batten et al., 1999; Joint et al., 2001), which we also see in our observations (Fig. 5; Table 2). Our estimated biomass was approximately twice as high as the long-term monthly mean (Batten et al., 1999; Joint et al., 2001) and higher than the biomass recorded between Mar 2014 and Mar 2015 at the E1 monitoring site 40 km south of Plymouth (app. 0.1–1.3 g DW m^{-2}) (Djeghri et al., this issue). Biomass composition and its spatial variability in April were also similar between our study and previous observations across the Celtic Sea (Fileman et al., 2011).

Our observation of warm temperatures (13.7 ± 0.4 °C) and high abundance of nauplii and copepodites in November is consistent with the observation that autumn blooms have continued into December in recent years (ICES, 2008). The composition of the mesozooplankton assemblage was much more diverse in November than during the other sampling periods with a large proportion of non-crustacean zooplankton, such as the larvae of starfish *Luidia sarsia,* salps (not

Table 4
Carbon-to-dry weight ratios (C:DW), isotopic signature and trophic positions (TP) for mesozooplankton in the Celtic Sea in 2014/2015. Early and late April refer to before and after the 19 April 2015. Values are mean ± SD.

Site	Season	Size class	C:DW (g:g)	$\delta^{15}N$ (‰)	TP (isotopic)	TP (biovolume spectra)
Central Site	November	200–500	0.43 ± 0.06	7.1 ± 0.2	3.6 ± 0.1	
		> 500	0.47 ± 0.13	7.9 ± 0.6	3.8 ± 0.2	4.5 ± 1.1
	Early April	200–500	0.45 ± 0.04	1.7 ± 0.7	1.7 ± 0.2	
		> 500	0.49 ± 0.02	2.3 ± 1.2	1.9 ± 0.3	2.4 ± 0.4
	Late April	200–500	0.43 ± 0.07	4.1 ± 0.5	1.9 ± 0.2	
		> 500	0.51 ± 0.03	3.6 ± 0.5	1.7 ± 0.1	4.1 ± 0.8
	July	200–500	0.46 ± 0.05	7.6 ± 0.9	2.4 ± 0.3	
		> 500	0.49 ± 0.02	7.8 ± 1.1	2.5 ± 0.3	2.4 ± 0.6
Shelf Edge	November	200–500	0.44 ± 0.03	5.9 ± 0.5	3.2 ± 0.2	
		> 500	0.38 ± 0.08	6.5 ± 0.7	3.4 ± 0.2	2.2 ± 0.3
	Early April	200–500	0.45 ± 0.02	0.6 ± 0.0	1.4 ± 0.0	
		> 500	0.48 ± 0.02	2.0 ± 0.3	1.8 ± 0.1	1.9 ± 0.3
	Late April	200–500	0.45 ± 0.06	2.0 ± NA	1.3 ± NA	
		> 500	NA	NA	NA	
	July	200–500	0.46 ± 0.04	7.6 ± 0.3	2.4 ± 0.1	
		> 500	0.47 ± 0.01	8.4 ± 0.4	2.6 ± 0.1	2.8 ± 0.1

Table 5
Results of NMDS and environmental variable fitting. NMDS1 and NMDS2 give vector directions. R^2 is the squared correlation coefficient. Significance levels (p-values)[a] are based on random permutations of the data. 'Daytime' was fitted as factor and has therefore no associated vector.

	NMDS 1	NMDS 2	R^2	p	
Longitude	−0.60	0.80	0.37	0.001	***
Day of year	−0.99	−0.10	0.24	0.007	**
Chl	0.34	−0.94	0.28	0.002	**
SST	0.10	0.99	0.37	0.001	***
Euphotic depth	0.88	−0.47	0.01	0.831	n.s.
Daytime			0.00	0.837	n.s.

[a] Statistical significance is indicated as $^{*}p < 0.05$, $^{**}p < 0.01$, $^{***}p < 0.001$, or not significant (n.s.).

quantitatively sampled due to very patchy abundance and inappropriate sampling gear), cnidarian, ctenophores, and the polychaete *Tomopteris*. This dominance by large predatory species supports the high trophic positions calculated from the biovolume spectra and isotopic composition (TP_{BVS} and TP_{iso}, respectively), with TP_{BVS} and TP_{iso} of lmZ being 4.5 ± 1.1 and 3.8 ± 0.2, respectively, at the Central Site (Table 4). These observations also agree well with long-term data from the Continuous Plankton Recorder, which suggest that chaetognaths, *Tomopteris* and coelenteran tissue (from ctenophores or cnidarians) persist in high abundance throughout the winter months (Johns, 2006). The high abundance of higher trophic levels in November is likely part of the typical prey-predator cycle in the Celtic Sea.

In early April, the microbial food web appeared to be well developed with long food chains leading to μP, as indicated by their high TP_{BVS} (3.3 ± 0.3 and 4.4 ± 0.4 at the Central Site and Shelf Edge, respectively; Fig. 8e and f, Supplementary Table 2). This matched the observation that the majority of primary production was by nanoplankton (Mayers et al., 2018), which is often associated with food chains dominated by small organisms and high recycling (Azam et al., 1983). Moreover, it has been suggested that ecosystems based on smaller phytoplankton likely have longer food chains and weak predator effects (Stibor et al., 2004).

Throughout April and July, we observed the typical increase in copepod biomass at both sites, which corresponds with the seasonality based on historical observations from the Continuous Plankton Recorder (Johns, 2006). *Calanus helgolandicus* has distinct peaks in abundance in the Celtic Sea region in June and October; *Para-Pseudocalanus* species demonstrate a similar seasonal pattern with a strong peak in May and a smaller secondary peak in the autumn months (Johns, 2006). These data (Johns, 2006) suggest that the population of calanoid copepods likely continues to increase after the spring bloom in April, which is also consistent with our observations that high biomass levels were maintained throughout July at both the Celtic Site and the Shelf Edge (Fig. 1; Note that overall biomass was lower at the Shelf Edge). Appendicularians, chaetognaths and euphausiids generally appear in late April (Fig. 5 and consistent with long-term data (Johns, 2006)), indicating a shift in the community structure towards a more developed food web. This is consistent with our observation of an increase of the trophic position (Fig. 8). Overall, our data show that the zooplankton communities at the Central Site and the Shelf Edge followed the expected pattern determined by long-term data (Johns, 2006).

4.2. Environmental drivers of seasonal progression

The ordination analysis identified 'seasonal ordination circles' for both the Central Site and the Shelf Edge (Fig. 6). Seasonal ordination circles are a graphic representation of the community cycle throughout the year, with distinct spring, autumn and winter communities. Distinct seasonal ordination circles, similar to ours (Fig. 6), have been observed for bacterial communities in the Mediterranean Sea (Erwin et al., 2012), phytoplankton communities in a deep subalpine lake (Salmaso, 1996), haptophytes in the Skagerrak (Egge et al., 2015), phytoplankton in the Western English Channel (Widdicombe et al., 2010), as well as mesozooplankton communities in the Mediterranean Sea (Cartes et al., 2008), temperate waters (Bode and Alvarez-Ossorio, 2004), and estuaries (Marques et al., 2009). The seasonal ordination circles for the Central Site and the Shelf Edge overlap for November, suggesting that the zooplankton communities were similar at both sites during this period. Thereafter, the circles diverge, highlighting different developments in the zooplankton communities at the two sites.

The ordination analysis suggests that the main environmental variables correlated with the seasonal community development are day of year (axis 1), and integrated Chl and sea surface temperature (axis 2; Fig. 6). Temperature and Chl appeared to have had opposing effects on community composition according to the NMDS (Fig. 6). A closer look at both variables showed that this was caused by temperature and Chl being negatively correlated (Supplementary Fig. 6). A similar negative relationship has been previously observed for the northeast Atlantic Ocean, including stations close to the Shelf Edge station (van de Poll et al., 2013). Indeed, our observed relationship (integrated Chl = 1603 ± 90 ∗ SST0.24 ± 0.03) is remarkably similar to theirs (int Chl = 1920 ∗ SST0.29) (van de Poll et al., 2013). The inverse relationship was likely driven by phytoplankton growth, which starts early in April when the water column starts stabilizing and the

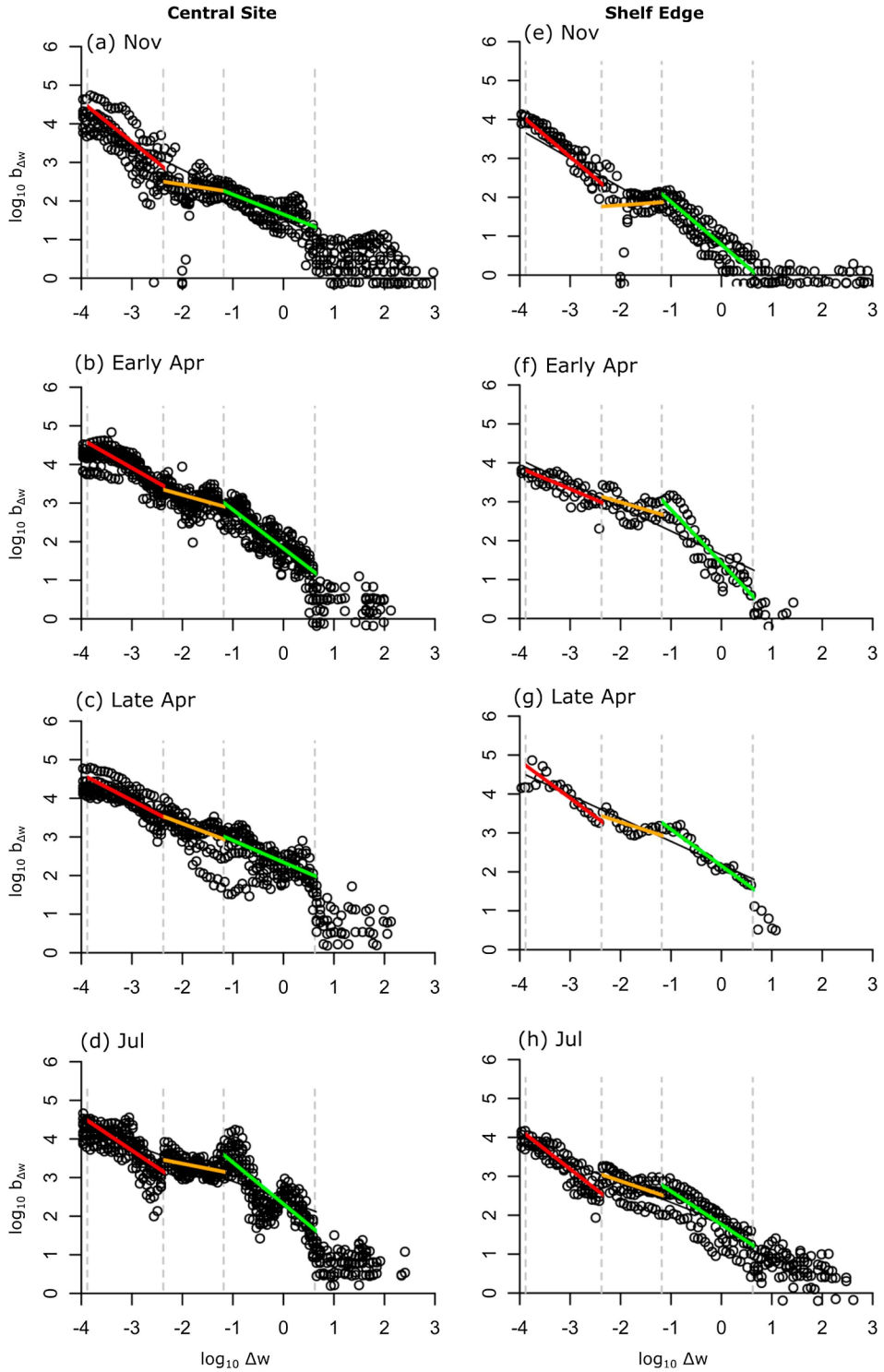

Fig. 7. Biovolume spectra at the Central Site (a–d) and the Shelf Edge (e and f) in November (a,e), early April (4–16 April; b,f), late April (20–28 Apr; c,g) and July (d,h).Slopes were fitted for large microplankton (μP, red line), small mesozooplankton (smZ, yellow line) and large mesozooplankton (lmZ, green line). Vertical dotted lines show the size cut off (63, 200, 500 and 2000 μm).

photoperiod becomes sufficiently long, resulting in relatively high Chl values before the water warms up. Later in the season, around July when the water reaches highest temperatures, low nutrient availability and top-down grazing keep phytoplankton biomass low, leading to high temperature and low Chl values.

The fact that day of year was identified as a driver highlights intrinsic seasonality in zooplankton life cycles. It also highlights that simple environmental parameters, such as temperature or Chl alone, are not sufficient to describe complex plankton communities and their seasonal development. Longitude (i.e. site) also emerged as a driver of community differences (Tables 5 and 6), suggesting that differences in the communities at the two sites were partly caused by site-specific environmental factors. These factors could be nutrient supply and/or predation pressure (see Section 4.4).

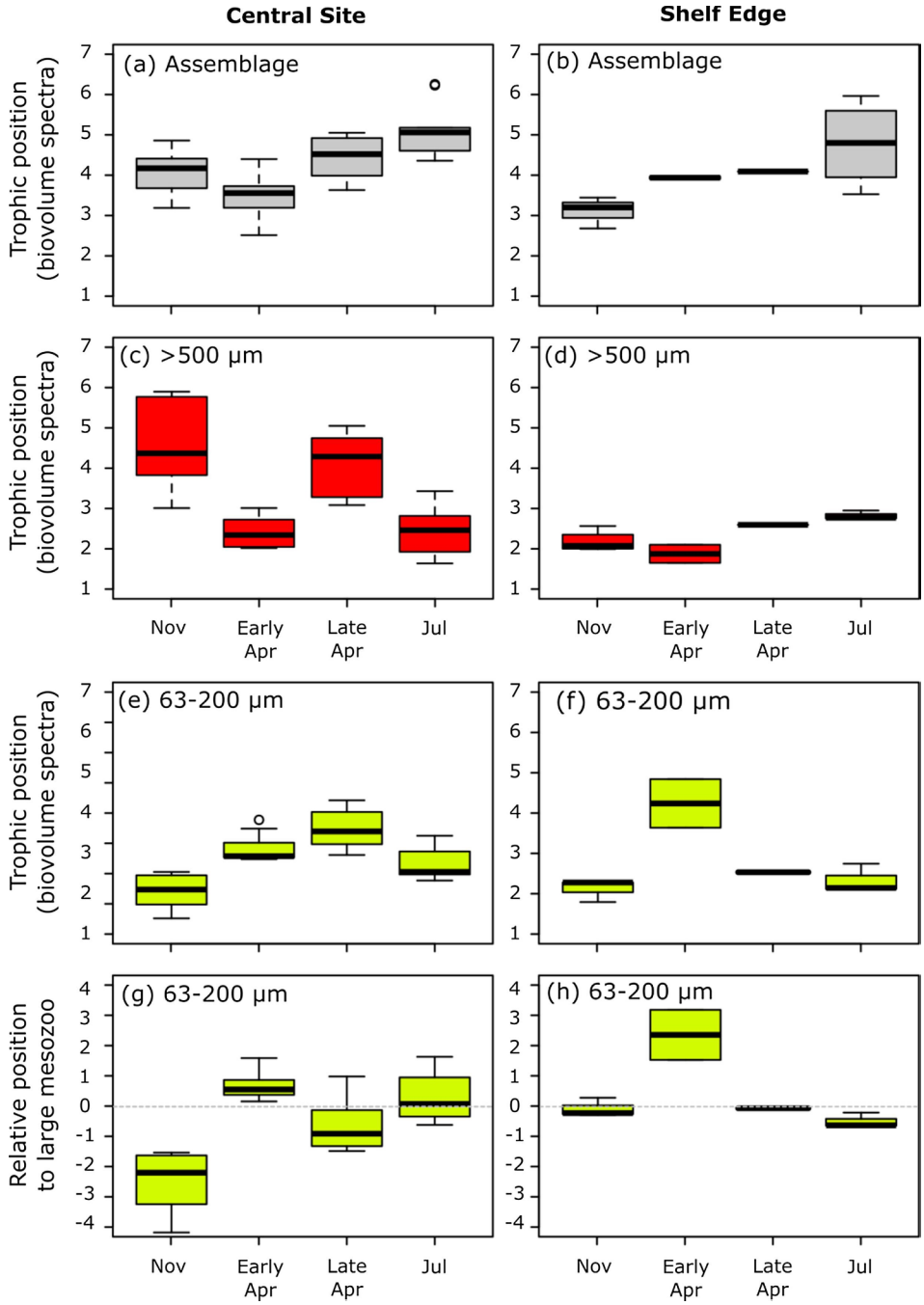

Fig. 8. Trophic positions of zooplankton in the Celtic Sea during four sampling periods. **(a–f)** Trophic position estimates based on biovolume spectra analysis for the whole assemblage (a,b), large mesozooplankton (lmZ, > 500 µm; c,d), and microplankton (µP, 63–200 µm; e,f). **(g–h)** Relative trophic position of µP to lmZ. Box plots show median, quartile range, minimum and maximum, and outliers. Trophic position was calculated for assemblages from the Central Site (left column) and Shelf Edge (right column).

4.3. Seasonal development of size spectra and trophic structure

All biovolume spectra in our study had slopes (−0.39 to −0.97, Supplementary Table 2) shallower than the theoretical prediction of a steady state system (−1.22) (Platt and Denman, 1978) and observed values for the North Atlantic near the Celtic Sea (−1.13 (San Martin et al., 2006)). Shallow slopes have also been observed in other regions, including, amongst others, in the Southwestern Atlantic Ocean (−0.2 to −0.9) (Thompson et al., 2013), the South China Sea (−0.67 to −0.93) (Zhou et al., 2015) and the Bay of Biscay (−0.2 to −1.4) (Vandromme et al., 2014). Comprehensive comparisons of spectra slopes have been compiled by (Dai et al., 2016; Sato et al., 2015), with values ranging from −0.44 to −2.30. It is noteworthy that these studies used a range of methods to estimate the spectra slopes (e.g. microscopy, the Laser Optical Plankton Counter, ZooScan or FlowCAM) and that absolute values for biovolume spectra slopes differ between methods. For example, spectra obtained using ZooScan are shallower than those obtained using the LOPC (Schultes and Lopes, 2009; Vandromme et al., 2014). As we applied the same methodology to all our biomass spectra, comparison and interpretation of our slopes at different sites and seasons is robust (Schultes and Lopes, 2009).

Seasonal changes in zooplankton size spectra have been observed in the Arctic and Antarctic shelves (Zhou et al., 2009). We suggest that our observations of shallow slopes and overall low biomass in November

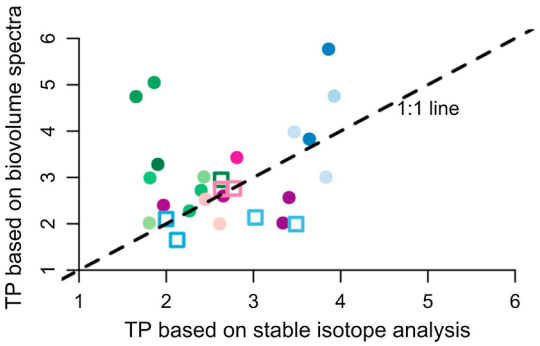

Fig. 9. Comparison between trophic position (TP) estimates based biovolume spectra analysis and stable isotope analysis. Only large mesozooplankton (lmZ) are compared. Symbols are coded according to sampling location (circle: Central Site; square: Shelf Edge) and sampling month (blue: November, green: April, purple: July; see legend in Fig. 2).

indicate an accumulation of biomass in the larger size classes, which were dominated by gelatinous zooplankton and large predatory species (Figs. 5 and 7). Such accumulation may be caused by the relatively high abundance of gelatinous zooplankton. In spring, steeper slopes indicate a shift to a community dominated by herbivorous zooplankton that are supported by the spring bloom (Fig. 10a). Towards the end of the summer, flatter slopes and an increased number of community trophic levels suggest either more recycling processes within the zooplankton community and a greater reliance upon the microbial loop and/or a change in the prey-predator size ratio towards more predators.

We also observed peaks and troughs in some of our biovolume spectra, which became more pronounced in late April and July at the Central Site (Fig. 7c and d). These anomalies may indicate predator-prey interactions (Sprules and Goyke, 1994; Thiebaux and Dickie, 1993), non-steady state conditions, cohort propagation (Edvardsen et al., 2002; Zhou, 2006), and/or a high abundance of a particular species (Zhou et al., 2009). Zhou et al. (2009), for example, noted that the dominance of *Calanus finmarchicus* on the Norwegian Shelf caused a distinct peak ('local maxima') at 1.5 mm^3 ($log_{10}\Delta w = 0.2$). During our study, *Calanus* spp. became increasingly abundant throughout April and dominated mesozooplankton biomass at the Central Site in late April and July (Fig. 5 and Supplementary Fig. 3), when we observed clear peaks at 0–0.5 $log_{10}\Delta w$ (Fig. 7c and d). We thus suggest that this particular peak is associated with the non-steady state of the Celtic Sea and caused by an increase in *Calanus* biomass.

Overall, we observed a close coupling between biomass and trophic position: community trophic position increased 1.1 TP per 10-fold increase in biovolume (Fig. 10d). This figure is surprisingly similar to the estimated community transfer efficiency of 10%, where – in an energy-limited system – a 10-fold increase in biomass allows the development of one additional trophic level (Pauly and Christensen, 1995; Pimm and Lawton, 1977). Alternatively, this relationship could also have been caused by accumulating biomass through seasonal growth and feeding (energy being passed up food web as the season progresses). A positive correlation between slopes and intercepts in zooplankton (Fig. 10c) was also observed across 25 lakes and the oligotrophic North Pacific (Sprules and Munawar, 1986), globally across the tropical and sub-tropical ocean (Mompeán et al., 2016) and around Japan (Sato et al., 2015). (Sprules and Munawar, 1986) showed that more productive systems, indicated by higher concentrations of total phosphorus and/or Chl, allow increased production of zooplankton biomass.

This trend is opposite to the observed negative correlation between slope (hence community trophic position) and biomass across the Bay of Biscay (Vandromme et al., 2014). A similar negative correlation was observed by (Marcolin et al., 2013) and (Dai et al., 2017). A possible explanation is that (Vandromme et al., 2014) and (Marcolin et al., 2013) sampled over a much larger area from near coast to the open

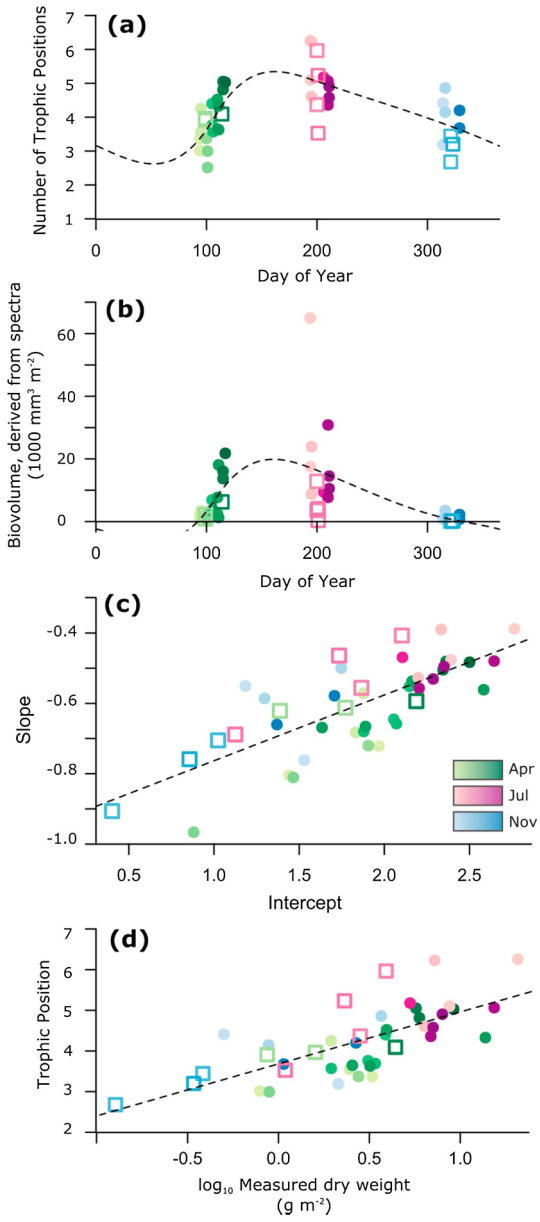

Fig. 10. Trophic community structure. **(a)** Seasonal time series of assemblage trophic positions throughout the study period based on biovolume spectrum analysis. Dotted line indicates the trend (fitted using cyclic spline smoother). **(b)** Seasonal time series of the total biovolume (derived from biomass spectra) throughout the study period. Dotted line indicates the trend (fitted using cyclic spline smoother). **(c)** Correlation between intercept and slope of all biovolume spectra. Line shows linear regression: $y = 0.19x - 0.95$ ($p < 0.01$, $R^2 = 0.56$, $n = 43$). **(d)** Correlation between assemblage trophic position based on biovolume spectra (TP_{BVS}) and measured dry weight (DW_m). Note log scale. Line shows regression line: $y = 1.06 \log_{10}(x)$.

ocean (> 2000 m depth), whilst (Dai et al., 2017) sampled across the mesopelagic and bathypelagic (0–3000 m depth). In addition, all three studies were carried out during only one season. These studies hence investigated a range of ecosystems with very different physical challenges. It has been shown that over a wide range of environments resource availability alone does not determine community trophic position, and other factors, such as disturbance and ecosystem size, play important roles in determining the food-chain length (Briand and Cohen, 1987; Post, 2002b). In the case of shelf-offshore transect (Marcolin et al., 2013; Vandromme et al., 2014), upwelling and increased turbulence at the shelf break and off-shore areas (as well as the

Table 6
Non-parametric MANOVA for community compositions at two sites (Central Site and Shelf Edge) during three months (November 2014, April 2015 and July 2015).[a]

	Degrees of freedom	Sum of squares	Mean squares	F	R^2	p	
Site	1	1.06	1.06	7.00	0.13	0.001	***
Month	1	0.96	0.96	6.34	0.12	0.001	***
Site*Month	1	0.31	0.31	2.06	0.04	0.084	.
Residuals	37	5.62	0.15		0.71		
Total	40	7.96			1		
Comparison[b]		p		Test for dispersion (p)		Tukey test (p)	
Central vs Shelf		0.001	***	0.30		0.29	
April vs July		0.001	***	0.10		0.09	
April vs November		0.001	***	0.88		0.87	
July vs November		0.001	***	0.22		0.22	

[a] Statistical significance is indicated as $^{*}p < 0.05$, $^{**}p < 0.01$ and $^{***}p < 0.001$. Otherwise p is stated.
[b] Pair-wise *a posteriori* tests. As significant differences in non-parametric MANOVAS can be caused by differences in dispersion, we tested for differences in dispersion and differences between mean distances (Tukey test).

upper water column) might favour an ecosystem based on fast-growing large diatom cells and a zooplankton community largely based on herbivory. The resulting biomass spectrum would have a high intercept and a steep slope. In contrast, on the shelf (or in the lower mesopelagic), the ecosystem is much more reliant on recycling processes and the microbial loop, leading to overall lower biomass (low intercept) and higher trophic levels. A study that samples over such contrasting environments would thus observe a negative relationship between biomass and trophic levels.

We conclude that our strong correlation between biomass and community trophic level is due to us sampling one relatively enclosed ecosystem throughout several seasons. Following the resource availability hypothesis (Pauly and Christensen, 1995; Pimm and Lawton, 1977), the increased energy input throughout April allowed the build-up of high biomass and overall more complex trophic community structure, followed by increased internal recycling during July, which maintained the trophic complexity (Hutchinson, 1959; Post, 2002b; Zhou, 2006). Overall, our biomass spectra suggest that the Celtic Sea is a relatively closed system and likely resource-limited during July.

4.4. Trophic coupling

Throughout our study, lmZ occupied trophic positions (TPs) between 1.7 and 4.5 (Table 4), which was similar to the trophic positions estimated for zooplankton across the North Atlantic in spring (Basedow et al., 2016). According to their study (Basedow et al., 2016), zooplankton between 600 and 4000 µm ESD occupied trophic positions between 2.1 and 5.8. Their and our trophic positions are higher than those commonly assigned to zooplankton, which are typically between 2 (herbivory) and 3 (carnivory) (Gascuel et al., 2011). Basedow et al. (2016) argued that high trophic positioning is, however, in line with our growing understanding of the complexity of planktonic food webs, including extensive recycling and linkages with the microbial loop (Azam et al., 1983; Mayor et al., 2014). For the North Atlantic, large copepods of the genus *Calanus* may occupy a trophic level of 5 if they feed on ciliates in a food web with particulate organic matter at the base and intense recycling by bacteria (Basedow et al., 2016). A similar conclusion can be drawn from the European Regional Seas Ecosystem Model (ERSEM) when the carbon flow follows the pathway: particulate/dissolved organic matter (TP 1) – bacteria (TP 2) – heterotrophs (TP 3) – microzooplankton (TP 4) – mesozooplankton (TP 5).

A similarly complex food chain would also explain the unusual observation that µP occupied a higher trophic level than lmZ during early April (Fig. 8g and h). The phytoplankton community in the Celtic Sea during this period was dominated by nanoplankton (Mayers et al., 2018). It is thus imaginable that µP fed on a mix of other smaller heterotrophic organisms, resulting in a trophic position of ~3. As these organisms may have been too small to be captured efficiently by lmZ (Berggreen et al., 1988), lmZ feeding could have been limited to the less abundant larger phytoplankton cells (> 20 µm) and microzooplankton, resulting in an overall lower trophic level (~2.5). Towards the end of April, smZ biomass increased (Supplementary Fig. 2). Grazing experiments performed as part of this research programme (Djeghri et al. this issue) show that lmZ grazed in proportion to the available food, suggesting that their prey composition changed. This is in agreement with the increased trophic position of lmZ towards the end of April (compared to early April, Fig. 8c and d; Table 4).

The Shelf Edge in July was characterized by a mesozooplankton community with much lower biomass and much higher diversity compared to the Central Site (Fig. 5), which is counterintuitive considering that the shelf break close to the Shelf Edge station is a productivity hotspot around July (Sharples et al., 2009, 2007). Owing to a vertical supply of nitrate by tidal mixing (Sharples et al., 2009, 2007), the distinct nutrient mixing regime at the shelf break favours a phytoplankton community dominated by large cells such as diatoms, which likely provide an important food source for large zooplankton (Sharples et al., 2013). This productivity causes a high abundance of fishes here, making the shelf break an important fishing ground (Sharples et al., 2013). We propose that the distinct zooplankton spring and summer communities at the Central Site and the Shelf Edge could have been caused by a combination of physical drivers (nutrient supply and lateral advection) (Palmer et al., this issue) and top-down control. The relatively low abundance of copepods at the Shelf Edge could have been caused by strong top-down control by predatory macrozooplankton and pelagic fishes, as also indicated by the drop off in the biovolume spectra (Fig. 7f and g) (Gislason, 1998; Perry et al., 2010).

Overall, our data suggest that the composition and trophic position of different size classes vary strongly over the year. Omnivorous feeding (Djeghri et al. this issue) and complex food webs challenge the conventional interpretation and categorization of zooplankton solely by size classes and functional types (Stowasser et al., 2012). Applying a single trophic position/functional type to a certain size class has the potential to misrepresent the role of zooplankton in the food web. A good example for this disparity is our data from April, during which lmZ initially had a lower trophic position than µP, but changed to a higher trophic position towards the end of the month owing to a shift in the composition of the available prey community. Basic food-web models that only include 2–3 types of zooplankton and focus on trophic interactions between species or size classes (e.g. microzooplankton vs mesozooplankton) are therefore likely to miss important flows of energy and matter through the ecosystem. Size-spectrum models provide an alternative as they track production and energy flows without an explicit description of each zooplankton type (Lefort et al., 2015). Moreover, they allow the projection of higher trophic levels. Size-spectrum models are therefore becoming increasingly popular and appear to be a promising tool for strategic management (Guiet et al., 2016; Jennings and Brander, 2010). The results of this study support the use of size spectra to infer trophic positions and their large potential for operational and monitoring studies, though current uncertainties in estimated trophic positions highlight the need of intercalibration with other methods such as taxonomy and stable isotopes.

Acknowledgements

We thank the captains, crews and scientists of the RRS Discovery cruises DY018, DY026, DY029 and DY033. We further thank S. Basedow for advice on biovolume spectra analysis. The work was funded by the UK Natural Environmental Research Council via the Shelf Sea Biogeochemistry research programme (NE/K002007/1 and NE/K002007/2) and through National Capability funding.

Appendix A. Supplementary material

Supplementary data associated with this article can be found, in the online version, at http://dx.doi.org/10.1016/j.pocean.2018.03.012.

References

Andersen, K.H., Berge, T., Gonçalves, R.J., Hartvig, M., Heuschele, J., Hylander, S., Jacobsen, N.S., Lindemann, C., Martens, E.A., Neuheimer, A.B., Olsson, K., Palacz, A., Prowe, A.E.F., Sainmont, J., Traving, S.J., Visser, A.W., Wadhwa, N., Kiørboe, T., 2016. Characteristic sizes of life in the Oceans, from Bacteria to Whales. Ann. Rev. Mar. Sci. 8, 217–241. http://dx.doi.org/10.1146/annurev-marine-122414-034144.

Anderson, M.J., 2001. A new method for non-parametric multivariate analysis of variance. Austral. Ecol. 26, 32–46. http://dx.doi.org/10.1111/j.1442-9993.2001.01070.pp. x.

Anderson, M.J., Ellingsen, K.E., McArdle, B.H., 2006. Multivariate dispersion as a measure of beta diversity. Ecol. Lett. 9, 683–693. http://dx.doi.org/10.1111/j.1461-0248.2006.00926.x.

Azam, F., Fenchel, T., Field, J., Gray, J., Meyer-Reil, L., Thingstad, F., 1983. The ecological role of water-column microbes in the sea. Mar. Ecol. Prog. Ser. 10, 257–263. http://dx.doi.org/10.3354/meps010257.

Basedow, S.L., de Silva, N.A.L., Bode, A., van Beusekorn, J., 2016. Trophic positions of mesozooplankton across the North Atlantic: estimates derived from biovolume spectrum theories and stable isotope analyses. J. Plankton Res. first publ. http://dx.doi.org/10.1093/plankt/fbw070.

Basedow, S.L., Tande, K.S., Zhou, M., 2010. Biovolume spectrum theories applied: spatial patterns of trophic levels within a mesozooplankton community at the polar front. J. Plankton Res. 32, 1105–1119. http://dx.doi.org/10.1093/plankt/fbp110.

Batten, S.D., Hirst, A.G., Hunter, J., Lampitt, R.S., 1999. Mesozooplankton biomass in the Celtic Sea: a first approach to comparing and combining CPR and LHPR data. J. Mar. Biol. Assoc. UK 79http://dx.doi.org/10.1017/S0025315497000209. S0025315497000209.

Berggreen, U., Hansen, B., Kiørboe, T., 1988. Food size spectra, ingestion and growth of the copepod Acartia tonsa during development: Implications for determination of copepod production. Mar. Biol. 99, 341–352. http://dx.doi.org/10.1007/BF02112126.

Blanchard, J.L., Heneghan, R.F., Everett, J.D., Trebilco, R., Richardson, A.J., 2017. From Bacteria to Whales: using functional size spectra to model marine ecosystems. Trends Ecol. Evol. 32, 174–186. http://dx.doi.org/10.1016/j.tree.2016.12.003.

Bode, A., Alvarez-Ossorio, M., 2004. Taxonomic versus trophic structure of mesozooplankton: a seasonal study of species succession and stable carbon and nitrogen isotopes in a coastal upwelling ecosystem. ICES J. Mar. Sci. 61, 563–571. http://dx.doi.org/10.1016/j.icesjms.2004.03.004.

Boyce, D.G., Frank, K.T., Leggett, W.C., 2015. From mice to elephants: overturning the "one size fits all" paradigm in marine plankton food chains. Ecol. Lett. 18, 504–515. http://dx.doi.org/10.1111/ele.12434.

Briand, F., Cohen, J.E., 1987. Environmental correlates of food chain length. Science 238, 956–960.

Burns, C.W., 1968. The relationship between body size of filter-feeding cladocera and the maximum size of particle ingested. Limnol. Oceanogr. 13, 675–678. http://dx.doi.org/10.4319/lo.1968.13.4.0675.

Carlotti, F., Poggiale, J.C., 2010. Towards methodological approaches to implement the zooplankton component in "end to end" food-web models. Prog. Oceanogr. 84, 20–38. http://dx.doi.org/10.1016/j.pocean.2009.09.003.

Caron, D.A., 2016. Mixotrophy stirs up our understanding of marine food webs. Proc. Natl. Acad. Sci. 113, 2806–2808. http://dx.doi.org/10.1073/pnas.1600718113.

Cartes, J.E., Madurell, T., Fanelli, E., López-Jurado, J.L., 2008. Dynamics of suprabenthos-zooplankton communities around the Balearic Islands (western Mediterranean): influence of environmental variables and effects on the biological cycle of Aristeus antennatus. J. Mar. Syst. 71, 316–335. http://dx.doi.org/10.1016/j.jmarsys.2006.11.013.

Dai, L., Li, C., Tao, Z., Yang, G., Wang, X., Zhu, M., 2017. Zooplankton abundance, biovolume and size spectra down to 3000 m depth in the western tropical North Pacific during autumn 2014. Deep Sea Res. Part I Oceanogr. Res. Pap. 121, 1–13. http://dx.doi.org/10.1016/j.dsr.2016.12.015.

Dai, L., Li, C., Yang, G., Sun, X., 2016. Zooplankton abundance, biovolume and size spectra at western boundary currents in the subtropical North Pacific during winter 2012. J. Mar. Syst. 155, 73–83. http://dx.doi.org/10.1016/j.jmarsys.2015.11.004.

Djeghri, N., Atkinson, A., Fileman, E.S., Harmer, R.A., Widdicombe, C.E., McEvoy, A.J., Cornwell, L., Mayor, D.J., 2018. High prey-predator size ratios and unselective feeding in copepods: a seasonal comparison of five species with contrasting feeding modes. Prog. Oceanogr. http://dx.doi.org/10.1016/j.pocean.2018.04.013. this issue.

Edvardsen, A., Zhou, M., Tande, K., Zhu, Y., 2002. Zooplankton population dynamics: measuring in situ growth and mortality rates using an Optical Plankton Counter. Mar. Ecol. Prog. Ser. 227, 205–219. http://dx.doi.org/10.3354/meps227205.

Edwards, A.M., Yool, A., 2000. The role of higher predation in plankton population models. J. Plankton Res. 22, 1085–1112. http://dx.doi.org/10.1093/plankt/22.6.1085.

Egge, E.S., Johannessen, T.V., Andersen, T., Eikrem, W., Bittner, L., Larsen, A., Sandaa, R.-A., Edvardsen, B., 2015. Seasonal diversity and dynamics of haptophytes in the Skagerrak, Norway, explored by high-throughput sequencing. Mol. Ecol. 24, 3026–3042. http://dx.doi.org/10.1111/mec.13160.

Erwin, P.M., Pita, L., Lopez-Legentil, S., Turon, X., 2012. Stability of sponge-associated bacteria over large seasonal shifts in temperature and irradiance. Appl. Environ. Microbiol. 78, 7358–7368. http://dx.doi.org/10.1128/AEM.02035-12.

Everett, J.D., Baird, M.E., Buchanan, P., Bulman, C., Davies, C., Downie, R., Griffiths, C., Heneghan, R., Kloser, R.J., Laiolo, L., Lara-Lopez, A., Lozano-Montes, H., Matear, R.J., McEnnulty, F., Robson, B., Rochester, W., Skerratt, J., Smith, J.A., Strzelecki, J., Suthers, I.M., Swadling, K.M., van Ruth, P., Richardson, A.J., 2017. Modeling what we sample and sampling what we model: challenges for zooplankton model assessment. Front. Mar. Sci. 4. http://dx.doi.org/10.3389/fmars.2017.00077.

Fileman, E.S., Fitzgeorge-Balfour, T., Tarran, G.A., Harris, R.P., 2011. Plankton community diversity from bacteria to copepods in bloom and non-bloom conditions in the Celtic Sea in spring. Estuar. Coast. Shelf Sci. 93, 403–414. http://dx.doi.org/10.1016/j.ecss.2011.05.009.

Friedland, K.D., Stock, C., Drinkwater, K.F., Link, J.S., Leaf, R.T., Shank, B.V., Rose, J.M., Pilskaln, C.H., Fogarty, M.J., 2012. Pathways between primary production and fisheries yields of large marine ecosystems. PLoS One 7, e28945. http://dx.doi.org/10.1371/journal.pone.0028945.

Gascuel, D., Guenette, S., Pauly, D., 2011. The trophic-level-based ecosystem modelling approach: theoretical overview and practical uses. ICES J. Mar. Sci. 68, 1403–1416. http://dx.doi.org/10.1093/icesjms/fsr062.

Giering, S.L.C., Cornwell, L., Fileman, E., Wells, S., Mayor, D.J., 2018. Plankton image details including abundance, sizing, identification and biomass estimates from the UK Shelf Sea during DY018, DY026A, DY029 and DY033. British Oceanographic Data Centre - Natural Environment Research Council, UK doi:10/cngc.

Gillooly, J.F., Brown, J.H., West, G.B., Savage, V.M., Charnov, E.L., 2001. Effects of size and temperature on metabolic rate. Science (80-.). 293, 2248–2251. http://dx.doi.org/10.1126/science.1061967.

Gislason, H., 1998. Modelling the response of size and diversity spectra of fish assemblages to changes in exploitation. ICES J. Mar. Sci. 55, 362–370. http://dx.doi.org/10.1006/jmsc.1997.0323.

Gonfiantini, R., 1978. Standards for stable isotope measurements in natural compounds. Nature 271, 534–536. http://dx.doi.org/10.1038/271534a0.

Gorsky, G., Ohman, M.D., Picheral, M., Gasparini, S., Stemmann, L., Romagnan, J.-B., Cawood, A., Pesant, S., Garcia-Comas, C., Prejger, F., 2010. Digital zooplankton image analysis using the ZooScan integrated system. J. Plankton Res. 32, 285–303. http://dx.doi.org/10.1093/plankt/fbp124.

Grosjean, P., Picheral, M., Warembourg, C., Gorsky, G., 2004. Enumeration, measurement, and identification of net zooplankton samples using the ZOOSCAN digital imaging system. ICES J. Mar. Sci. 61, 518–525. http://dx.doi.org/10.1016/j.icesjms.2004.03.012.

Guiet, J., Poggiale, J.-C., Maury, O., 2016. Modelling the community size-spectrum: recent developments and new directions. Ecol. Modell. 337, 4–14. http://dx.doi.org/10.1016/j.ecolmodel.2016.05.015.

Heneghan, R.F., Everett, J.D., Blanchard, J.L., Richardson, A.J., 2016. Zooplankton are not fish: improving zooplankton realism in size-spectrum models mediates energy transfer in food webs. Front. Mar. Sci. 3. http://dx.doi.org/10.3389/fmars.2016.00201.

Hopcroft, R.R., Roff, J.C., Chavez, F.P., 2001. Hydrobiologia 453 (454), 133–141. http://dx.doi.org/10.1023/A:1013167917679.

Hutchinson, G.E., 1959. Homage to Santa Rosalia or why are there so many kinds of animals? Am. Nat. 93, 145–159. http://dx.doi.org/10.1086/282070.

Hyder, K., Rossberg, A.G., Allen, J.I., Austen, M.C., Barciela, R.M., Bannister, H.J., Blackwell, P.G., Blanchard, J.L., Burrows, M.T., Defriez, E., Dorrington, T., Edwards, K.P., Garcia-Carreras, B., Heath, M.R., Hembury, D.J., Heymans, J.J., Holt, J., Houle, J.E., Jennings, S., Mackinson, S., Malcolm, S.J., McPike, R., Mee, L., Mills, D.K., Montgomery, C., Pearson, D., Pinnegar, J.K., Pollicino, M., Popova, E.E., Rae, L., Rogers, S.I., Speirs, D., Spence, M.A., Thorpe, R., Turner, R.K., van der Molen, J., Yool, A., Paterson, D.M., 2015. Making modelling count - increasing the contribution of shelf-seas community and ecosystem models to policy development and management. Mar. Policy 61, 291–302. http://dx.doi.org/10.1016/j.marpol.2015.07.015.

ICES, 2008. Report of the ICES Advisory Committee 2008, ICES Advice 2008. Copenhagen.

Jennings, S., Brander, K., 2010. Predicting the effects of climate change on marine communities and the consequences for fisheries. J. Mar. Syst. 79, 418–426. http://dx.doi.org/10.1016/j.jmarsys.2008.12.016.

Johns, D., 2006. The Plankton Ecology of SEA 8 area. Sir Alistair Hardy Foundation for Ocean Science, Plymouth.

Joint, I., Wollast, R., Chou, L., Batten, S., Elskens, M., Edwards, E., Hirst, A., Burkill, P., Groom, S., Gibb, S., Miller, A., Hydes, D., Dehairs, F., Antia, A., Barlow, R., Rees, A., Pomroy, A., Brockmann, U., Cummings, D., Lampitt, R., Loijens, M., Mantoura, F., Miller, P., Raabe, T., Alvarez-Salgado, X., Stelfox, C., Woolfenden, J., 2001. Pelagic production at the Celtic Sea shelf break. Deep Sea Res. Part II. Top. Stud. Oceanogr. 48, 3049–3081. http://dx.doi.org/10.1016/S0967-0645(01)00032-7.

Kiørboe, T., 2013. Zooplankton body composition. Limnol. Oceanogr. 58, 1843–1850. http://dx.doi.org/10.4319/lo.2013.58.5.1843.

Lefort, S., Aumont, O., Bopp, L., Arsouze, T., Gehlen, M., Maury, O., 2015. Spatial and

body-size dependent response of marine pelagic communities to projected global climate change. Glob. Chang. Biol. 21, 154–164. http://dx.doi.org/10.1111/gcb.12679.
Legendre, P., Legendre, L., 1998. Numerical ecology, second Englis. ed. Elsevier, Amsterdam.
Lehette, P., Hernández-León, S., 2009. Zooplankton biomass estimation from digitized images: a comparison between subtropical and Antarctic organisms. Limnol. Oceanogr. Methods 7, 304–308. http://dx.doi.org/10.4319/lom.2009.7.304.
Levin, L.A., Liu, K.-K., Emeis, K.-C., Breitburg, D.L., Cloern, J., Deutsch, C., Giani, M., Goffart, A., Hofmann, E.E., Lachkar, Z., Limburg, K., Liu, S.-M., Montes, E., Naqvi, W., Ragueneau, O., Rabouille, C., Sarkar, S.K., Swaney, D.P., Wassman, P., Wishner, K.F., 2015. Comparative biogeochemistry–ecosystem–human interactions on dynamic continental margins. J. Mar. Syst. 141, 3–17. http://dx.doi.org/10.1016/j.jmarsys.2014.04.016.
Marcolin, C. da R., Schultes, S., Jackson, G.A., Lopes, R.M., 2013. Plankton and seston size spectra estimated by the LOPC and ZooScan in the Abrolhos Bank ecosystem (SE Atlantic). Cont. Shelf Res. 70, 74–87. http://dx.doi.org/10.1016/j.csr.2013.09.022.
Marques, S.C., Azeiteiro, U.M., Martinho, F., Viegas, I., Pardal, M.A., 2009. Evaluation of estuarine mesozooplankton dynamics at a fine temporal scale: the role of seasonal, lunar and diel cycles. J. Plankton Res. 31, 1249–1263. http://dx.doi.org/10.1093/plankt/fbp068.
Marquis, E., Niquil, N., Vezina, A.F., Petitgas, P., Dupuy, C., 2011. Influence of planktonic foodweb structure on a system's capacity to support pelagic production: an inverse analysis approach. ICES J. Mar. Sci. 68, 803–812. http://dx.doi.org/10.1093/icesjms/fsr027.
Mayor, D.J., Sanders, R., Giering, S.L.C., Anderson, T.R., 2014. Microbial gardening in the ocean's twilight zone: Detritivorous metazoans benefit from fragmenting, rather than ingesting, sinking detritus. BioEssays 36, 1132–1137. http://dx.doi.org/10.1002/bies.201400100.
Mayers, K.M.J., Poulton, A.J., Daniels, C.J., Wells, S.R., Woodward, E.M.S., Tarran, G.A., Widdicombe, G.A., Mayor, D.J., Atkinson, A., Giering, S.L.C., 2018. Growth and mortality of coccolithophores during spring in a temperate Shelf Sea (Celtic Sea, April 2015). Prog. Oceanogr. http://dx.doi.org/10.1016/j.pocean.2018.02.024. (in press).
Minagawa, M., Wada, E., 1984. Stepwise enrichment of 15N along food chains: further evidence and the relation between δ15N and animal age. Geochim. Cosmochim. Acta 48, 1135–1140. http://dx.doi.org/10.1016/0016-7037(84)90204-7.
Mitra, A., Castellani, C., Gentleman, W.C., Jónasdóttir, S.H., Flynn, K.J., Bode, A., Halsband, C., Kuhn, P., Licandro, P., Agersted, M.D., Calbet, A., Lindeque, P.K., Koppelmann, R., Møller, E.F., Gislason, A., Nielsen, T.G., St. John, M., 2014. Bridging the gap between marine biogeochemical and fisheries sciences; configuring the zooplankton link. Prog. Oceanogr. 129, 176–199. http://dx.doi.org/10.1016/j.pocean.2014.04.025.
Mompeán, C., Bode, A., Latasa, M., Fernández-Castro, B., Mouriño-Carballido, B., Irigoien, X., 2016. The influence of nitrogen inputs on biomass and trophic structure of ocean plankton: a study using biomass and stable isotope size-spectra. J. Plankton Res. 38, 1163–1177. http://dx.doi.org/10.1093/plankt/fbw052.
O'Boyle, S., Silke, J., 2010. A review of phytoplankton ecology in estuarine and coastal waters around Ireland. J. Plankton Res. 32, 99–118. http://dx.doi.org/10.1093/plankt/fbp097.
Oksanen, J., Blanchet, F.G., Friendly, M., Kindt, R., Legendre, P., McGlinn, D., Minchin, P. R., O'Hara, R.B., Simpson, G.L., Solymos, P., Stevens, M.H.H., Szoecs, E., Wagner, H., 2016. vegan: Community Ecology Package.
Pauly, D., Christensen, V., 1995. Primary production required to sustain global fisheries. Nature 374, 255–257. http://dx.doi.org/10.1038/374255a0.
Perry, R.I., Cury, P., Brander, K., Jennings, S., Möllmann, C., Planque, B., 2010. Sensitivity of marine systems to climate and fishing: concepts, issues and management responses. J. Mar. Syst. 79, 427–435. http://dx.doi.org/10.1016/j.jmarsys.2008.12.017.
Pimm, S., Lawton, J., 1977. Number of trophic levels in ecological communities. Nature 268, 329–331.
Pingree, R.D., Holligan, P.M., Mardell, G.T., Head, R.N., 1976. The influence of physical stability on spring, summer and autumn phytoplankton blooms in the Celtic Sea. J. Mar. Biol. Assoc. United Kingdom 56, 845. http://dx.doi.org/10.1017/S0025315400020919.
Platt, T., Denman, K., 1977. Organisation in the pelagic ecosystem. Helgoländer Wissenschaftliche Meeresuntersuchungen 30, 575–581. http://dx.doi.org/10.1007/BF02207862.
Platt, T., Denman, K.L., 1978. The structure of pelagic marine ecosystems. Rapp. ProceÂs-Verbaux Des ReÂunions - Cons Perm. Int. Pour L'exploration La Mer 173, 60–65.
Post, D.M., 2002a. Using stable isotopes to estimate trophic position: models, methods, and assumptions. Ecology 83, 703–718. http://dx.doi.org/10.1890/0012-9658(2002) 083[0703:USITET]2.0.CO;2.
Post, D.M., 2002b. The long and short of food-chain length. Trends Ecol. Evol. 17, 269–277. http://dx.doi.org/10.1016/S0169-5347(02)02455-2.
Qi, H., Coplen, T.B., Geilmann, H., Brand, W.A., B?hlke, J.K., 2003. Two new organic reference materials for d13 C and d15 N measurements and a new value for the d13 C of NBS 22 oil. Rapid Commun. Mass Spectrom. 17, 2483–2487. http://dx.doi.org/10.1002/rcm.1219.
R Core Team, 2015. R: A Language and Environment for Statistical Computing.
Salmaso, N., 1996. Seasonal variation in the composition and rate of change of the phytoplankton community in a deep subalpine lake (Lake Garda, Northern Italy). An application of nonmetric multidimensional scaling and cluster analysis. Hydrobiologia 337, 49–68. http://dx.doi.org/10.1007/BF00028506.
San Martin, E., Harris, R.P., Irigoien, X., 2006. Latitudinal variation in plankton size spectra in the Atlantic Ocean. Deep Sea Res. Part II. Top. Stud. Oceanogr. 53, 1560–1572. http://dx.doi.org/10.1016/j.dsr2.2006.05.006.
Sato, K., Matsuno, K., Arima, D., Abe, Y., Yamaguchi, A., 2015. Spatial and temporal changes in zooplankton abundance, biovolume, and size spectra in the neighboring waters of Japan: analyses using an optical plankton counter. Zool. Stud. 54, 18. http://dx.doi.org/10.1186/s40555-014-0098-z.
Schultes, S., Lopes, R.M., 2009. Laser Optical Plankton Counter and Zooscan intercomparison in tropical and subtropical marine ecosystems. Limnol. Oceanogr. Methods 7, 771–784. http://dx.doi.org/10.4319/lom.2009.7.771.
Sharples, J., Moore, C.M., Hickman, A.E., Holligan, P.M., Tweddle, J.F., Palmer, M.R., Simpson, J.H., 2009. Internal tidal mixing as a control on continental margin ecosystems. Geophys. Res. Lett. 36, L23603. http://dx.doi.org/10.1029/2009GL040683.
Sharples, J., Scott, B.E., Inall, M.E., 2013. From physics to fishing over a shelf sea bank. Prog. Oceanogr. 117, 1–8. http://dx.doi.org/10.1016/j.pocean.2013.06.015.
Sharples, J., Tweddle, J.F., Mattias Green, J.A., Palmer, M.R., Kim, Y.-N., Hickman, A.E., Holligan, P.M., Moore, C.M., Rippeth, T.P., Simpson, J.H., Krivtsov, V., 2007. Spring-neap modulation of internal tide mixing and vertical nitrate fluxes at a shelf edge in summer. Limnol. Oceanogr. 52, 1735–1747. http://dx.doi.org/10.4319/lo.2007.52.5.1735.
Silvert, W., Platt, T., 1978. Energy flux in the pelagic ecosystem: a time-dependent equation. Limnol. Oceanogr. 23, 813–816. http://dx.doi.org/10.4319/lo.1978.23.4.0813.
Sommer, F., 2004. 15N signatures of marine mesozooplankton and seston size fractions in Kiel Fjord, Baltic Sea. J. Plankton Res. 26, 495–500. http://dx.doi.org/10.1093/plankt/fbh048.
Sommer, U., Sommer, F., 2006. Cladocerans versus copepods: the cause of contrasting top–down controls on freshwater and marine phytoplankton. Oecologia 147, 183–194. http://dx.doi.org/10.1007/s00442-005-0320-0.
Sprules, W.G., Goyke, A.P., 1994. Size-based structure and production in the Pelagia of Lakes Ontario and Michigan. Can. J. Fish. Aquat. Sci. 51, 2603–2611. http://dx.doi.org/10.1139/f94-260.
Sprules, W.G., Munawar, M., 1986. Plankton size spectra in relation to ecosystem productivity, size, and perturbation. Can. J. Fish. Aquat. Sci. 43, 1789–1794. http://dx.doi.org/10.1139/f86-222.
Steinberg, D.K., Landry, M.R., 2017. Zooplankton and the Ocean Carbon Cycle. Ann. Rev. Mar. Sci. 9, 413–444. http://dx.doi.org/10.1146/annurev-marine-010814-015924.
Stibor, H., Vadstein, O., Diehl, S., Gelzleichter, A., Hansen, T., Hantzsche, F., Katechakis, A., Lippert, B., Løseth, K., Peters, C., Roederer, W., Sandow, M., Sundt-Hansen, L., Olsen, Y., 2004. Copepods act as a switch between alternative trophic cascades in marine pelagic food webs. Ecol. Lett. 7, 321–328. http://dx.doi.org/10.1111/j.1461-0248.2004.00580.x.
Stowasser, G., Atkinson, A., McGill, R.A.R., Phillips, R.A., Collins, M.A., Pond, D.W., 2012. Food web dynamics in the Scotia Sea in summer: a stable isotope study. Deep Sea Res. Part II. Top. Stud. Oceanogr. 59, 208–221. http://dx.doi.org/10.1016/j.dsr2.2011.08.004.
Tarling, G.A., Stowasser, G., Ward, P., Poulton, A.J., Zhou, M., Venables, H.J., McGill, R.A.R., Murphy, E.J., 2012. Seasonal trophic structure of the Scotia Sea pelagic ecosystem considered through biomass spectra and stable isotope analysis. Deep Sea Res. Part II. Top. Stud. Oceanogr. 59–60, 222–236. http://dx.doi.org/10.1016/j.dsr2.2011.07.002.
Thiebaux, M.L., Dickie, L.M., 1993. Structure of the body-size spectrum of the biomass in aquatic ecosystems: a consequence of allometry in predator-prey interactions. Can. J. Fish. Aquat. Sci. 50, 1308–1317. http://dx.doi.org/10.1139/f93-148.
Thompson, G.A., Dinofrio, E.O., Alder, V.A., 2013. Structure, abundance and biomass size spectra of copepods and other zooplankton communities in upper waters of the Southwestern Atlantic Ocean during summer. J. Plankton Res. 35, 610–629. http://dx.doi.org/10.1093/plankt/fbt014.
van de Poll, W.H., Kulk, G., Timmermans, K.R., Brussaard, C.P.D., van der Woerd, H.J., Kehoe, M.J., Mojica, K.D.A., Visser, R.J.W., Rozema, P.D., Buma, A.G.J., 2013. Phytoplankton chlorophyll a biomass, composition, and productivity along a temperature and stratification gradient in the northeast Atlantic Ocean. Biogeosciences 10, 4227–4240. http://dx.doi.org/10.5194/bg-10-4227-2013.
Vandromme, P., Nogueira, E., Huret, M., Lopez-Urrutia, Á., González-Nuevo González, G., Sourisseau, M., Petitgas, P., 2014. Springtime zooplankton size structure over the continental shelf of the Bay of Biscay. Ocean Sci. 10, 821–835. http://dx.doi.org/10.5194/os-10-821-2014.
Visser, A., Fiksen, Ø., 2013. Optimal foraging in marine ecosystem models: selectivity, profitability and switching. Mar. Ecol. Prog. Ser. 473, 91–101. http://dx.doi.org/10.3354/meps10079.
Warren, P.H., Lawton, J.H., 1987. Invertebrate predator-prey body size relationships: an explanation for upper triangular food webs and patterns in food web structure? Oecologia 74, 231–235. http://dx.doi.org/10.1007/BF00379364.
Widdicombe, C.E., Eloire, D., Harbour, D., Harris, R.P., Somerfield, P.J., 2010. Long-term phytoplankton community dynamics in the Western English Channel. J. Plankton Res. 32, 643–655. http://dx.doi.org/10.1093/plankt/fbp127.
Williams, R., Collins, N.R., 1986. Seasonal composition of meroplankton and holoplankton in the Bristol Channel. Mar. Biol. 92, 93–101. http://dx.doi.org/10.1007/BF00392751.
Williams, R., Conway, D.V.P., 1982. Population growth and vertical distribution of calanus helgolandicus in the celtic sea. Netherlands J. Sea Res. 16, 185–194. http://dx.

doi.org/10.1016/0077-7579(82)90029-1.
Wood, S.N., 2017. Generalized Additive Models: An Introduction with R, second ed. Chapman and Hall/CRC Press.
Woodward, G., Ebenman, B., Emmerson, M., Montoya, J., Olesen, J., Valido, A., Warren, P., 2005. Body size in ecological networks. Trends Ecol. Evol. 20, 402–409. http://dx.doi.org/10.1016/j.tree.2005.04.005.
Zhou, L., Huang, L., Tan, Y., Lian, X., Li, K., 2015. Size-based analysis of a zooplankton community under the influence of the Pearl River plume and coastal upwelling in the northeastern South China Sea. Mar. Biol. Res. 11, 168–179. http://dx.doi.org/10.1080/17451000.2014.904882.
Zhou, M., 2006. What determines the slope of a plankton biomass spectrum? J. Plankton Res. 28, 437–448. http://dx.doi.org/10.1093/plankt/fbi119.
Zhou, M., Tande, K.S., Zhu, Y., Basedow, S., 2009. Productivity, trophic levels and size spectra of zooplankton in northern Norwegian shelf regions. Deep Sea Res Part II Top. Stud. Oceanogr. 56, 1934–1944. http://dx.doi.org/10.1016/j.dsr2.2008.11.018.